Aalto-yliopisto
Aalto-universitetet
Aalto University

Master’s Program in Energy Storage

Thermal characterisation of a Power to Methanol reactor

Paweł Winiarski

Master’s Thesis
2022

Aalto-yliopisto
Aalto-universitetet
Aalto University

Author Paweł Winiarski

Title of thesis Thermal characterisation of a Power to Methanol reactor

Programme Master's in Energy Storage

Thesis supervisor Prof. Stefania Specchia

Thesis advisor(s) Prof. Annukka Santasalo-Aarnio, Dr Arpad Toldy

Date 09.07.2022 **Number of pages** 56 + 15 **Language** English

Abstract

Synthetic methanol produced from CO_2 and H_2 is one of the technical solutions necessary to combat anthropogenic climate change. It can replace fossil fuel feedstocks currently used in the chemical industry and be used as an alternative fuel in some types of engines and turbines. Because of this, methanol synthesis has recently gained increased attention from researchers of industry and academia.

This thesis covers the topic of heat transfer in a laboratory scale power to methanol reactor, which was built with the purpose to investigate different catalysts and working conditions for synthetic methanol production. The design and construction of the reactor setup was a subject of a previous master thesis. The focus of this thesis is computational fluid dynamics (CFD) modelling of transient heat transfer in a fixed bed catalytic reactor with a simplistic and effective approach. The experimental setup is shortly introduced, and the experimental methods of early stage reactor operation are presented.

Calibrating a CFD model with experimental data is a further part of this thesis, the aim of which is to achieve representative simulation accuracy. Afterwards, the results from measurements are presented. The CFD model is used to recreate the experiments, with the intention to extrapolate preceding temperature results to the whole reactor volume.

After calibration, the model achieved sufficiently low simulation error of reactor's bed temperature (< 10°C), both in steady state and transient operation. With that, its readiness to aid future experiment planning and ensuring safety of operation has been achieved. Methanol % yield of steady state operation was estimated as 8.6%.

Keywords Methanol, E-methanol, Synthetic fuel, Thermal Analysis, Heat transfer, Experimental Reactor, Laboratory Scale, Carbon Dioxide, Hydrogen.

Contents

Preface

I want to thank Professor Annukka Santasalo-Aarnio for guidance and giving me the opportunity to work in her team on this master thesis. This was a special experience for me to join a group of experienced, enthusiastic and friendly researchers contributing to advances in energy transition. I thank Professor Stefania Specchia for advice I received during the development of my methods and results. I am grateful to Doctor Arpad Toldy for his contribution to building up my understanding of engineering concepts. I also want to express my gratitude towards Markus Laitinen, with whom I was collaborating through a half-year journey of experimental research.

I am immensely grateful to my partner Marta, who spurred me into studying abroad and gave me endless love and support throughout this time. I want to thank my parents Violetta and Adam for encouragement they were giving me during that journey. I thank my brothers Michał and Rafał, for always being my inspiration.

I want to express my gratitude towards Finnish and Italian education systems for high quality education, which my peers and I have received throughout our master studies. Last, but not least, I want to thank European Union for allowing me to study a leading double degree master's program and for taking the lead in global climate action.

Otaniemi, 9 July 2022
Paweł Winiarski

The thesis is written as part of a collaborative joint degree programme called Master's Programme in Energy Storage (EIT InnoEnergy).

Aalto University is responsible for the implementation of the programme along with Politecnico di Torino (PoliTo) and EIT InnoEnergy, a knowledge and innovation community of the European Institute of Innovation and Technology.

The thesis is supervised by both partner universities.

Symbols and abbreviations

Symbols

ρ	density
t	time
v	velocity vector
g	gravitational force field vector
p	pressure
μ	fluid dynamic viscosity
μ'	fluid dynamic viscosity secondary term for complex molecules
X	vector of mass fraction of different chemical species
$\vert v \vert$	absolute value of velocity
h	vector of specific enthalpies of separate chemical species
D_{ij}	binary diffusion coefficients between different chemical species
M_j	molar weight of chemical species j
R	a vector of rate of production of chemical species
Y	molar weight
ϕ	concentration of a physical quantity
q	volumetric source term
n	a vector normal to surface
r	rate of chemical reaction
k_{eff}	forward rate constant of reaction
C_X	concentration of reactant X
A_{eff}	preexponential factor
E_{eff}	effective activation energy
R	gas constant
T	absolute temperature
a, b	reaction order
h	Planck constant
$\dot{q}$	external heat
$v_{reactants}$	volumetric flow rate of reactants
δT	measurement uncertainty of temperature
δp	measurement uncertainty of pressure
$\delta Tsim$	measurement uncertainty of simulated temperature
$p_{decrease}$	pressure decrease
vol_{fluid}	reactor internal void space available for fluid
$ratio_{MeOH}$	ratio of molecules of MeOH produced to total molecules attributing to volume decrease in CO_2 hydrogenation reaction
v_{MeOH}	volumetric rate of produced MeOH
ΔH	reaction enthalpy
$\%Yield$	per cent yield of a reaction towards a selected species
Q_{MeOH}	total reaction heating power generated from CO_2 hydrogenation
$Q_{MeOH+RWGS}$	total reaction heating power

$\boldsymbol{Q_{RWGS}}$	total reaction heating power generated from RWGS reaction
$\boldsymbol{c_{fb}}$	coefficient of heat transfer between process fluid and fixed bed particles
$\boldsymbol{c_{bo}}$	coefficient of heat transfer between fixed bed particles and cooling oil
$\boldsymbol{c_{oe}}$	coefficient of heat transfer between cooling oil and environment
$\boldsymbol{c_{bet}}$	coefficient of heat transfer between fixed bed particles and environment through top lid
$\boldsymbol{c_{beb}}$	coefficient of heat transfer between fixed bed particles and environment through bottom lid

Operators

$\nabla^*\mathbf{A}$	divergence of vector **A**
$\nabla \mathrm{B}$	gradient of scalar B
$\Delta\mathbf{A}$	laplacian of vector **A**
$\nabla \times \mathbf{A}$	curl of vector **A**
$\frac{\partial}{\partial t}$	partial derivative with respect to variable t
$\sum_{j=1}^{N}$	sum over index i until maximum value N
$\oiint_{\partial Vc=S}$	surface integral over area S, which is also a boundary of volume V_c
$\oiiint_{Vc}$	volume integral over volume V_c
$\prod_{j}$	repeated multiplication over index j
$\Delta\widehat{G_i}$	change of variable of state G_i from reactant to transition state

Abbreviations

CFD	Computational Fluid Dynamics
DFT	Density Functional Theory
FVM	finite volume method
GC	gas chromatograph
LHHW	Langmuir-Hinshelwood-Hougen-Watson kinetics
MASI	most abundant surface intermediate
MFC	mass flow controller
RTD	resistance temperature detectors
RWGS	reverse water-gas shift reaction

1 Introduction

Mitigation of climate change is the biggest challenge of human civilisation in XXI century. Climate change is caused by greenhouse gas emissions originating from utilisation of fossil fuels [1]. To end the demand of fossil fuels, the development of a variety of highly advanced technical solutions is required, along with targeted carbon taxes across all the sectors of economy [2]. Two of these sectors are power industry and chemical industry [3]. In the case of the former, the power systems require the capability of ramping up and down the level of power supply. This means utilisation of flexible power sources, such as gas turbines and engines powered by alternative sustainable fuels [4]. When it comes to chemical industry, sustainable feedstock fuels are also needed to cut down on both greenhouse gas emissions and fossil fuel dependence [5]. This would enable production of climate friendly alternatives for many products, such as textiles, polymers, paints, fertilisers or pharmaceuticals [6] [7].

Synthetic methanol (e-methanol) is a chemical compound, which is going to have an enormous relevance in addressing the sustainable fuel demand in the following decades [8] [9] [10] [11]. It is produced through synthesis of two reactants: carbon dioxide and hydrogen, and the reaction is usually carried out in a fixed bed reactor [12]. There are, nevertheless, certain sustainability conditions related to sourcing of these gases. Firstly, hydrogen needs to be obtained from water electrolysis process powered by low-carbon electricity. Secondly, in order for e-methanol to qualify as sustainable, it needs to follow the circular economy concept, in which the carbon atoms circulate between being components of methanol, components of end products made from methanol and components of carbon dioxide [13]. Such carbon atoms should never end up in the atmosphere. To achieve this circularity, carbon dioxide needs to be captured either directly from the atmosphere or from the same industrial point source, which is going to utilise later such recycled methanol.

Methanol demand is estimated for 500Mt annually in 2050 [11]. Synthesis of e-methanol is already a commercial process, with several companies, including Carbon Recycling International and Fairway Methanol, already producing it volumes and planning further development into hundreds thousands of tons yearly [14] [15]. Despite the fact of existing production, there is room for improvements in the process technology, with the ultimate goal of bringing down the production costs and allowing for rapid global scale up of e-methanol. One of such possible process improvements is using a new type of catalyst for the chemical reaction and the second one is optimizing the reaction conditions inside the reactor [12]. These efforts have potential to increase the reaction yield, causing a decrease of the costs of auxiliary energy demand related to product gas separation [16].

With the aim to test such improved processes, researchers conduct tests in different scales. One of the necessary test phases is a laboratory scale (bench scale) process evaluation, for which the construction of experimental reactor setup is needed. In parallel, computational modelling of the reactor internal space is a common practice. The intention of such modelling is to better understand the physical phenomena occurring in the reactor, as well as to optimize the conditions inside the reactor. Since the 1990s, researchers have been using computational fluid dynamics (CFD) as a tool in reactor modelling and many methods were established and improved since then [17]. The modelling usually includes heat and mass transfer, as well as reactions of chemical species. The level of detail in these chemical reaction models can be very precise, to the stage when every catalyst particle of the reactor bed is reproduced with its exact shape and position [18]. However, simulations based on such models not only require high computational performance, but also a significant amount of effort and cost for the development process. In many cases that is not necessary, as less specific results are representative with enough level of accuracy.

With newly designed chemical laboratory scale reactors, it is practical to model their behaviour during transient operation, such as start-up and shutdown. However, simulating such operation with a sophisticated CFD model is a massively time-demanding procedure. Because of that, there might be a preference for easy to implement, simplistic models, which would return results with lower, but still valuable level of precision. This thesis presents a new CFD model for studying transient operation of a laboratory scale e-methanol synthesis reactor, which had been built in Aalto University. Besides the development of the computational model, also results of multiple experiments are presented, including measurements of pressure and temperature during different stages of operation of the reactor. Based on these methods, the thesis intends to answer the following research questions:

1. What is the thermal behaviour of the Power to methanol reactor during different stages of operation?

2. Is it possible to calibrate a heat transfer model of the Power to methanol reactor with sufficient accuracy to achieve simulation results comparable with experimental data?

3. What is the yield of reaction products during steady state operation of the Power to methanol reactor?

The main outcomes of the thesis are the results of model validation with experimental data. The observations of heat transfer and chemical reactions occurring in the reactor during transient operation are also included. The presented results can help researchers to assess if simplistic CFD modelling could be an aid in their future work with laboratory scale chemical reactors.

2 CFD modelling of fixed bed reactors

Chemical reactors are the main components of chemical plants, where the desired reactions take place. One of reactor types used widely in large-scale industrial production of chemicals and intermediates is a catalytic fixed bed (packed bed) reactor [19]. In these reactors, internal space is filled with particles of specifically chosen size and shape, which are usually porous and have their surface covered with a specific catalyst. The role of a fixed bed is to provide large surface area for the catalytic reactions to take place, converting reactants into products. A schematic of a fixed bed reactor is illustrated in Figure 1.

Figure 1: A fixed bed reactor. Source: [19].

Most of chemical reactors operate at steady state conditions during long-term production runs. In such runs, small variations in product yield can lead into significant financial loss for the production plant. Therefore, it is key to maintain optimal reaction conditions of the reactor, including desired pressure and temperature. In cases of highly exothermic or endothermic reactions taking place in isothermal reactors, there is a requirement for effective heat transfer between catalyst and circulating heat transfer medium. One of the most common setups of a fixed bed reactor is a multi-tubular fixed bed reactor, where the catalyst is packed into neighbouring tubes, which are cooled by a stream of heat transfer medium [20]. A schematic of a multi-tubular fixed bed is presented in Figure 2.

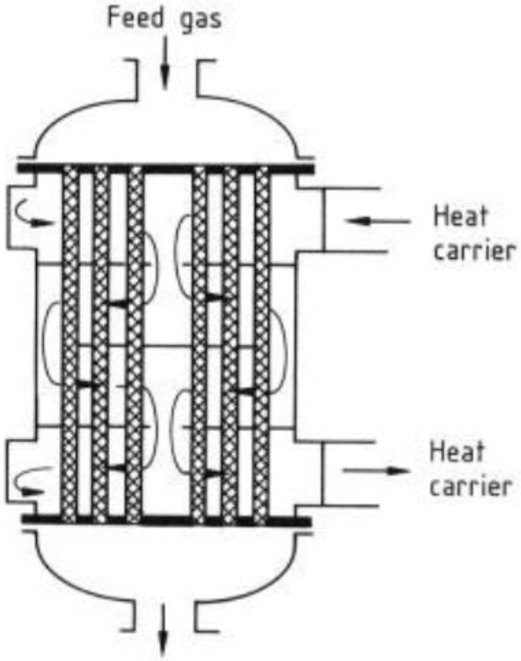

Figure 2: A multitubular fixed bed reactor. Source: [19].

In such type of reactor, effective heat transfer is ensured by tubes of small diameter, each of them working as a separated fixed bed, instead of having a bulk fixed bed in the whole reactor area. These tubes have a higher specific heat transfer area than a bulk reactor and ensure easier temperature control, and by result, easier selectivity control [21]. The following requirement of a fixed bed is to maintain low pressure drop along the flow of process gas. This requirement is in favour of larger catalyst particles, while heat and mass transfer is more effective with smaller catalyst particles due to them having higher surface area. Because of these conflicting goals, reactors beds need to be assembled in a way to provide a middle ground for optimal results [17]. Low pressure drop is especially important in case of chemical reactions characterised by low single pass conversion, in which the use of product recirculation is necessary. This is because product recirculation implies significant energy losses, which should be minimised where possible. Because of these matters, reactor setups with a small tube-to-particle diameter ratio are often preferred [22].

Due to significant influence of fluid dynamic phenomena on reaction conversion, it is of interest of both industry and academia to research into possible improvements of the fixed bed reactors. Computational modelling enables the investigation of possible improvements of reactor layout, as well as optimal reactor conditions [23]. The areas of these improvements include bed morphology, pressure drop, mixing characteristics, heat and mass transfer and surface chemistry.

2.1 Geometry of a fixed bed

With the aim to meet all the requirements related to heat transfer, mass transfer and pressure drop, many types of catalyst arrangements have been proposed for fixed bed configurations. The catalyst may be in the form of random packings of particles, such as spheres, solid and hollow cylinders, as well as monolithic shapes with parallel channels, stacked plates or corrugated-plate packets [19]. In general, beds with random packing provide good reaction surface area with supreme mixing conditions, which allows minimising the mass transport resistance between gas and catalyst surface. The resulting turbulence in inter-particle area is an important factor. Such turbulence improves greatly convective heat transfer from the bed, despite low heat conductivity of gases compared to solid particle material [24].

In many cases, there is no need to develop a computational model with a high level of complexity, due to practical reasons. CFD simulations of fixed bed reactors are often carried out with modelling assumption of quasi-homogeneous (single-phase) bed [25] [26]. Such assumption implies that the fixed bed is a continuous medium with averaged properties of packing and void space. The temperature of the process fluid and the surrounding particle is therefore always equal and heat transfer properties of such a single phase, called effective properties, have the averaged values of its two-phase components [27]. The underlying simplicity of implementation of quasi-homogeneous models, as well as sufficient accuracy and reliability allows to utilisation of these models in many applications [28]. Another way to model a fixed bed is heterogeneous (double phase) modelling approach [29], [30], [31]. Such models take into consideration the co-existence of solid medium of the particles together with void space, allowing the two media to exchange heat and mass between them and maintain different temperatures. A group of researchers concluded, that in steady state conditions the results obtained by homo and heterogeneous models are similar [32].

With continuous advances in computational modelling, researchers are interested in development of models of higher accuracy than homo or heterogeneous approach [33] [34] [35] [36]. This is possible with a method of single particle modelling, which is also called three-dimensional (3D) particle-resolved modelling. The difference between particle-resolved and heterogeneous methods is that in the prior the solid phase is not considered a continuum medium, but rather a dispersed phase, with separate thermal conditions at each separate particle. A comparison of these models is illustrated in Figure 3.

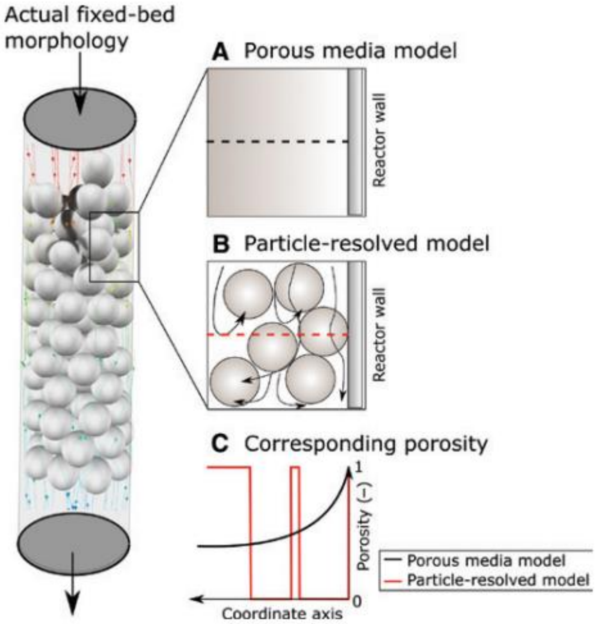

Figure 4: A difference in morphology between a homogeneous bed model and a particle-resolved model of a fixed-bed reactor. Source: [22].

In order to model reactors with small tube-to-particle ratio, particle-resolved models are the only choice with sufficient accuracy level. This is because both homo and heterogeneous models do not include local inter-particle and intra-particle phenomena, such as turbulence, mass transport, unequal velocity profiles across particles or the existence of hot and cold spots in the catalyst bed.

Particle-resolved CFD modelling requires the creation of fixed bed packing geometry with a very high level of detail. There are different ways to obtain such a geometry, including tomography of a real reactor, regular generation and random generation of the bed geometry using software [37] [38]. The latter is highly important, when the catalyst particles do not have spherical shape – such as cylinders [39]. Such cylindrical pellets would never assume regular distribution inside a fixed bed, so a dedicated algorithm is necessary to generate a representative arrangement of these particles. In literature, there were many reports of algorithms dedicated to generation of such bed geometries [40], [41], [42], as well as experiments leading to validation of the algorithms [43].

One of the biggest challenges in particle-resolved modelling fixed bed reactors is representation of the contacts between different particles. The presence of contact points, lines and sometimes areas leads to severe convergence errors in the simulations, along local anomalies in fluid flow as well as heat and mass transfer. Researchers explored solutions to address these issues, usually by combining geometrical simplifications of particle shapes [44].

The most popular shape simplifications are the caps method and the bridges method [22]. Both of these simplifications are local geometry modifications, affecting only areas of inter-particle contact and particle-wall contact. Their role is to make it easy for the CFD model to compute balance equations, by reducing geometry and mesh complexity. The bridges method relies on placing a small extrusion-like connection between the contact points, while the caps method is the opposite, as it subtracts the volume of the particles in the close distance from the contact points. Geometry changes resulting from these methods are presented in Figure 5, which shows an example of two cylindrical catalyst particles and a wall. Both of these techniques have their advantages and disadvantages. The bridges method tends to overestimate heat transfer between objects in contact, while the caps method has a tendency to underestimate heat transfer, while overestimating the fluid flow through the void space of the bed [45]. After the geometry of a modelled component is created, the next step is the discretization of such geometry into a mesh of finite elements or volumes.

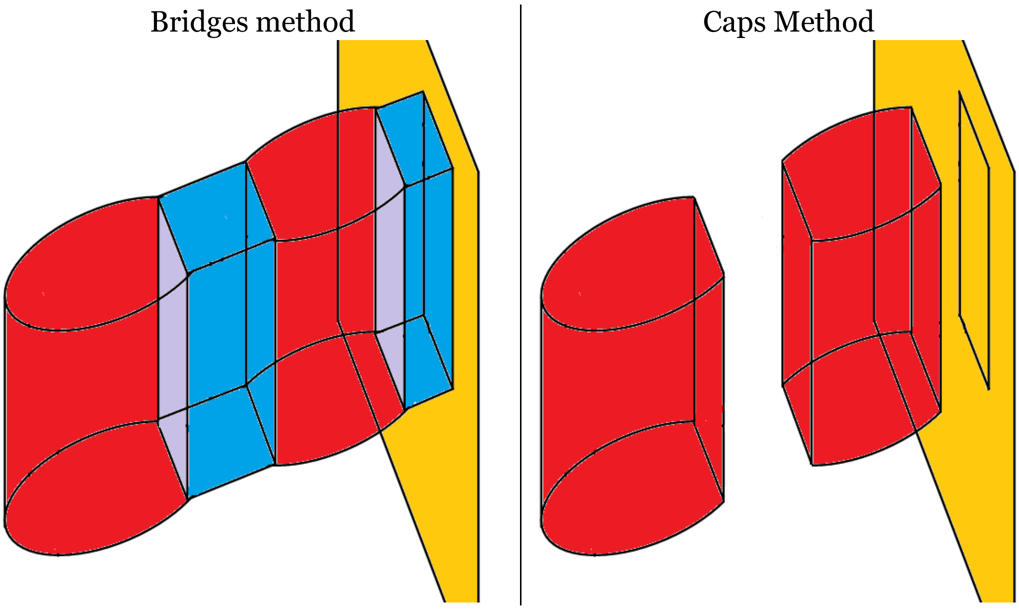

Figure 5: Two methods of modification of contact point geometry for two cylindrical catalyst particles and a wall.

2.2 Governing balance equations

In order to develop a representative CFD model, all physical phenomena need to be expressed with a set of equations. For a chemical reactor, these equations include balance of mass, momentum, energy and mass of chemical species. The equations are presented below.

Mass balance:

$$\frac{\partial \rho}{\partial t} + \nabla * (\rho \boldsymbol{v}) = 0 \tag{1}$$

where:
$\rho - \mathit{fluid\ density},$ $\boldsymbol{v} - \mathit{fluid\ velocity\ vector}.$

Momentum balance in vector form:

$$\rho\left(\frac{\partial \boldsymbol{v}}{\partial t} + \boldsymbol{v}(\nabla * \boldsymbol{v})\right) = \rho \boldsymbol{g} - \nabla p + \mu \Delta \boldsymbol{v} + \left(\frac{\mu}{3} + \mu'\right) * \nabla(\nabla * \boldsymbol{v}) \tag{2}$$

where:
$\rho - \mathit{fluid\ density},$ $\boldsymbol{v} - \mathit{fluid\ velocity\ vector},$
$\boldsymbol{g} - \mathit{gravitational\ force\ field\ vector},$ $p - \mathit{pressure\ field},$
$\mu - \mathit{fluid\ dynamic\ viscosity},$
$\mu' - \mathit{fluid\ dynamic\ viscosity\ secondary\ term\ for\ complex\ molecules}$

Energy balance:

$$\begin{aligned} &\rho \frac{\partial}{\partial t}\left(\frac{|v|^2}{2} + h\right) = \rho(\boldsymbol{g} * \boldsymbol{v}) - \nabla * (p\boldsymbol{v}) + \\ &+\nabla * \left(\mu * \nabla(|v|^2) - \mu \boldsymbol{v} * (\nabla \times \boldsymbol{v}) + \left(\mu' - \frac{2}{3}\mu\right)\boldsymbol{v} * (\nabla * \boldsymbol{v})\right) + \\ &+\nabla * \left[-k\nabla T + \boldsymbol{h} * \nabla \boldsymbol{X} * (-\rho) * \left(\frac{1 - Y_i}{\sum_{j \neq i}^{N} \frac{Y_j}{D_{ij}}}\right)\right] = \dot{Q} \end{aligned} \tag{3}$$

where:
$\boldsymbol{X} = \frac{m_i}{m} - \mathit{a\ vector\ of\ mass\ fraction\ of\ different\ species}\ (i = 1,2,\dots,N),$
$\rho - \mathit{fluid\ density},$ $\boldsymbol{v} - \mathit{fluid\ velocity\ vector},$
$\boldsymbol{g} - \mathit{gravitational\ force\ field\ vector},$ $p - \mathit{pressure},$

$|v| - absolute\ value\ of\ fluid\ velocity,$
$\mu - fluid\ dynamic\ viscosity,$ $h - specific\ enthalpy$ of a mixture
$\mu' - fluid\ dynamic\ viscosity\ secondary\ term\ for\ complex\ molecules,$
$\boldsymbol{h} - vector\ of\ specific\ enthalpies\ of\ separate\ chemical\ species,$
$\dot{Q} - heat\ generation\ source\ term,$
$D_{ij} - binary\ diffusion\ coefficients\ between\ different\ species,$
and molar weight Y of the species i is described as:

$$Y_i = \frac{1}{\sum_{j=1}^{N} \frac{X_j}{M_j}} \frac{X_i}{M_i} \tag{4}$$

where M_j is the molar weight of species j.

Mass balance of chemical species:

$$\rho\left(\frac{\partial \boldsymbol{X}}{\partial t} + \boldsymbol{v} * \nabla \boldsymbol{X}\right) + \nabla * \left(-\rho * \nabla \boldsymbol{X} * \left(\frac{1 - Y_i}{\sum_{j \neq i}^{N} \frac{Y_j}{D_{ij}}}\right)\right) = \boldsymbol{R} \tag{5}$$

where:

$\boldsymbol{X} = \frac{m_i}{m} - a\ vector\ of\ mass\ fraction\ of\ different\ species\ (i = 1,2,\dots,N),$
$\rho - fluid\ density,$ $\boldsymbol{v} - fluid\ velocity\ vector,$
$\boldsymbol{R} - a\ vector\ of\ rate\ of\ production\ of\ chemical\ species,$
and molar weight Y of the species i is described as:

$$Y_i = \frac{1}{\sum_{j=1}^{N} \frac{X_j}{M_j}} \frac{X_i}{M_i} \tag{6}$$

Finite Volume Method (FVM) is a leading technique of CFD modelling for variety of applications, which include also modelling of fixed bed reactors [22]. It relies on discretization of the volume of analyzed component into a mesh of finite, non-overlapping volumes [46] and discretisation of complex differential equations of balance into relatively simple algebraic form for each mesh volume (cell). This creates a large system of equations, which is solvable in steady state, given enough boundary conditions at external surfaces. For transient simulations, additional information is needed in the form of initial conditions of each variable for which the time-dependent solution is looked for. Figure 6: shows an example of a 2D hexahedral mesh element with sources and fluxes of any given physical quantity. This quantity could be mass, momentum, energy or mass of chemical species. This chapter provides only the brief description of the FVM method, as the full explanation would exceed the volume of this thesis. An interested reader is encouraged to look into the exhaustive literature available on the topic [46].

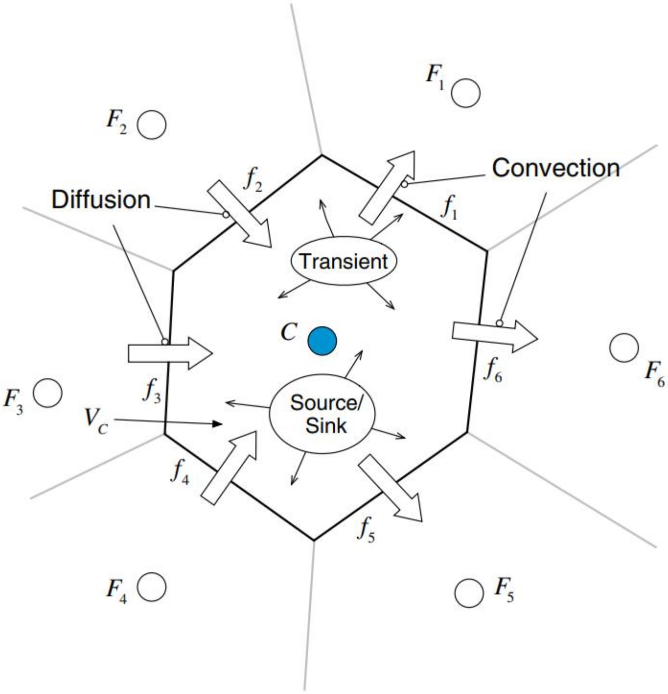

Figure 6: A 2D hexahedral mesh element with sources and fluxes of a given physical quantity.

FVM is inherently conservative, which means that all the physical quantities, including mass, momentum and energy are always conserved along the mesh of finite volumes by the nature of the model. This is due to the fact that the surfaces of mesh cells are used as flux areas for transport of physical quantities, such as mass or energy, and the flux entering a particular cell from a given direction is always equal to flux leaving the adjacent cell from the same direction. Another advantage of FVM is that the unknown quantity is always evaluated in the bulk of the cell, instead of in its surface, which makes it easy to implement various surface boundary conditions. When it comes to mesh type in particle-resolved simulations, in the literature the most accurate modelling results were obtained using polyhedral mesh cells, as they were less vulnerable to numerical diffusion than other types of mesh cells, while being more precise in areas of complex fluid flow [47].

After choosing of governing equations and a numerical method, the next step is the discretization process, in which the balance equations are discretized (or integrated) over the finite volumes (mesh elements). The general term for any conservation equation in its integral form can be presented as:

$$\oiiint_{Vc} \rho \frac{\partial \phi}{\partial t}\, dV + \oiint_{\partial Vc=S} \rho \phi \boldsymbol{v} * \boldsymbol{n} dS = \oiint_{\partial Vc=S} \Gamma \nabla \phi * \boldsymbol{n}\, dS + \oiiint_{Vc} q\, dV \tag{7}$$

where:
$\rho - fluid\ density, \qquad \phi - intensive\ physical\ quantity,$
$\boldsymbol{v} - fluid\ velocity\ vector, \qquad q - volumetric\ source\ term\ ,$
$\boldsymbol{n} - a\ vector\ normal\ to\ surface\ S\ of\ a\ finite\ volume\ Vc.$
$\Gamma - diffusive\ parameter\ for\ diffusion\ of\ \phi.$

This equation is valid for each finite volume, as well as for the whole domain. To obtain the result of such integration, surfaces as well as volumes of each cell need to be calculated. Convective and diffusive fluxes across all cell surfaces are transformed using the Gauss theorem (8), which allows to transform volume integrals into surface integrals. This ultimately leads to the solution of the discreet equations over each element.

$$\oiint_{\partial Vc=S} \boldsymbol{f} * \boldsymbol{n}\, dS = \sum_{i=1}^{n} (\boldsymbol{f} * \boldsymbol{n_i}) * S_i = \oiiint_{Vc} (\nabla * \boldsymbol{f})\, dV \tag{8}$$

where:
$\boldsymbol{f} - a\ flux\ field\ vector\ for\ any\ given\ physical\ quantity,$
$\boldsymbol{n} - a\ vector\ normal\ to\ surface\ S\ of\ a\ finite\ volume\ Vc.$

The last steps are expressing the quantity fluxes – diffusive and convective – in terms of the difference of quantity values of adjacent cells, as well as providing boundary conditions on external boundaries of the component. Afterwards, a system of algebraic equations is obtained and it is possible to be solved.

2.3 Chemical reactions

In majority of cases of chemical reactions occurring in fixed bed reactors, the reactions happen mostly at the surface of catalyst particles. However, there are additional necessary steps for a chemical reaction to take place, such as transport of the molecule from bulk of the fluid to the catalyst surface, as well as the other way around after the reaction is finished. In general, 7 different steps can be distinguished for each molecule taking part in a chemical reaction:

1. Transport from the fluid to the catalyst surface
2. Transport from the catalyst surface through a pore to the reaction site
3. Surface adsorption
4. Surface reaction
5. Surface desorption
6. Transport from the reaction site through a pore to the catalyst surface
7. Transport from the catalyst surface to the fluid

The computational methods covering steps 3-5 are called microkinetic models. There are also conjugate approaches including all the steps 1-7, which are named macrokinetic models.

Two typical engineering objective of a chemical reaction is to achieve a high reactant conversion and a decent reaction rate. These two parameters are the main indicators about the reaction performance. Literature provides different pathways for modelling of the reaction rates [48]. One of these pathways is power-law kinetics, which was years ago the most common type of expression for reaction rate (I). Power-law kinetics is a closed-form empirical kinetic model, which means that the coefficients present in the equation are estimated based on experimental results.

$$r = k_{eff} C_A^a C_B^b = A_{eff} e^{-\frac{E_{eff}}{RT}} C_A^a C_B^b \tag{I}$$

where:
$r - rate\ of\ reaction,$
$k_{eff} - forward\ rate\ constant\ of\ reaction,$
$C_X - concentration\ of\ reactant\ X,\quad A_{eff} - preexponential\ factor,$
$E_{eff} - effective\ activation\ energy,\ R - gas\ constant,$
$T - absolute\ temperature,\qquad a, b - reaction\ order.$

Despite the limitations of power-law kinetic approach, it is still commonly used in both in reactor design and process design due to its simplicity and possibility of straight-forward regression based on experimental data.

Another way of modelling rate of reaction is Langmuir-Hinshelwood-Hougen-Watson (LHHW) kinetics [22]. In LHHW models, the surface mechanisms are described with a high level of detail. Additionally, there are incorporated assumptions on slow and fast reaction steps. One of the underlying assumptions is that adsorption-desorption processes are in partial equilibrium. Further requirement is to choose manually the rate determining step of reaction. Similarly, to power-law kinetics, the LHHW model needs to be fitted with experimental data in order to create a representative description of reaction rate. If the modelling results are in good correlation with experimental ones, e.g., the conversion and selectivity data, the rate constants are fixed at the corresponding values.

Because of procedures mentioned above, LHHW is inherently subjected to many uncertainties, such as measurement or modelling uncertainties. For example, even if model reproduces the data with satisfying accuracy, it may be due to a coincidence of two simultaneous errors. Consequently, the resulting reaction rate is prone to uncertainty propagation. Other examples include inability of the model to predict the most abundant surface intermediate (MASI), which is responsible for blocking catalyst sites, or the effective reaction orders. Even if practically correct in a range of operating conditions, the reaction rate coefficients obtained with LHHW often show no physical significance other than being a numerical parameter built into the model.

Mean-field approximation is the third method of estimation of reaction rates. Unlike power-law approach, it is not regressed into a narrow range of experimental conditions, making it more universal. It includes elementary reactions, which opens the possibility to investigate reaction intermediates and reaction rates. What is also an important advantage, it allows for estimation of sensitivity of certain model parameters.

This kind of model assumes the uniform distribution of adsorbate and catalyst sites at the surface. The reaction rate of elementary, irreversible reaction is outlined with the following equation:

$$r_i = k_i \prod_j c_j = A_i \exp\left(-\frac{\Delta E_i}{k_B T}\right) \prod_j c_j \qquad \text{(II)}$$

where:
$k_i -$ *forward rate constant of reaction i,*
$c_j -$ *concentration of reactant j,* $A_i -$ *preexponential factor,*
$\Delta E_i -$ *activation energy,* $k_B -$ *Boltzmann constant,*
$T -$ *absolute temperature.*

The rate constant is assumed independent of local conditions of the reaction’s location. A modified form of this equation, originating from transition state theory (TST), refers the rate constant to Gibbs free energy of reactants, products and transition states [48]:

$$k_i = \frac{k_B T}{h} \exp\left(-\frac{\Delta \widehat{G_i}}{k_B T}\right) = \frac{k_B T}{h} \exp\left(\frac{\Delta \hat{S}}{k_B}\right) \exp\left(\frac{-\Delta \widehat{H_i}}{k_B T}\right) \qquad \text{(III)}$$

where:
$k_i -$ *forward rate constant of reaction i,*
$k_B -$ *Boltzmann constant,* $T -$ *absolute temperature,*
$h -$ *Planck constant,*
$\Delta \widehat{G_i} -$ *change of Gibbs free energy from reactant to transition state,*
$\Delta \hat{S} -$ *change of entropy from reactant to transition state,*
$\Delta \widehat{H_i} -$ *change of enthalpy from reactant to transition state.*

Additionally, the reaction equilibrium constant can be calculated in relation to Gibbs free energy:

$$K_i = \exp\left(-\frac{\Delta \mathrm{G_i}}{k_B T}\right) = \exp\left(\frac{\Delta}{k_B}\right) \exp\left(\frac{-\Delta H_i}{k_B T}\right) \qquad \text{(IV)}$$

where:
$K_i -$ *equilibrium constant of reaction i,*
$\Delta \mathrm{G_i} -$ *change of Gibbs free energy of reaction i,*
$\Delta S_i -$ *change of entropy of reaction i,*
$\Delta H_i -$ *change of entalphy of reaction i.*
$k_B -$ *Boltzmann constant,* $T -$ *absolute temperature.*

In recent years, it became possible to estimate some parameters, such as activation energies of adsorbates, using semi-empirical methods, which are not only simple in implementation, but also have a higher level of accuracy when compared to empirical methods. This is a major improvement, since with the early days of kinetic modelling, the rate constants could only be determined with fitting them empirically to experimental results. The semi-empirical method returns good quality results with small molecules. The most precise and in-depth level of modelling can be achieved with a microkinetic method called Density Functional Theory (DFT). The description of DFT is outside of the scope of this thesis. An interested reader is encouraged to look into available literature [49] [50].

In general, methanol synthesis is described by 3 chemical reactions [51]:

$$CO + 2H_2 \leftrightarrow CH_3OH \quad \left(\Delta°H = -\frac{91kJ}{mol}\right) \tag{V}$$

$$CO_2 + 3H_2 \leftrightarrow CH_3OH + H_2O \quad \left(\Delta°H = -\frac{49.5kJ}{mol}\right) \tag{VI}$$

$$CO + 2H_2 \leftrightarrow CH_3OH \quad \left(\Delta°H = -\frac{91kJ}{mol}\right) \tag{VII}$$

The reactions depicted by equations (V) (VI) (VII) are called consecutively CO hydrogenation, CO_2 hydrogenation and reverse water-gas shift (RWGS).

Reactor kinetic models of methanol synthesis through CO_2 hydrogenation have been described and compared by researchers in both steady state and transient conditions [52]. In the same study, the kinetics of methanol synthesis was also reported, along with assumptions and schemes of implementation. However, the kinetics and exact pathway of production of methanol are still a matter of scientific discussion, despite many studies dedicated to these problems. The existing LHHW kinetic models differ between each other about the source of carbon atoms for methanol molecule. Some of the studies assume that only carbon monoxide takes part in the hydrogenation reaction [53] [54], while others consider only carbon dioxide [55] [56], and some assume that both pathways happen in parallel [57] [58].

CO_2 has been demonstrated to be the main reactant in methanol synthesis [59], while other study showed that CO_2 restrains CO hydrogenation, but not its own hydrogenation to methanol. These observations led to a hypothesis of separate catalyst sites being responsible for CO and CO_2 hydrogenation. This was further supported by different experiments [60]. Graaf et. al. proposed a model where separate catalyst sites are responsible for CO/CO_2 and H_2/H_2O adsorption. [57] [61]. They suggested that CO and CO_2 hydrogenation takes place consecutively, afterwards being followed by RWGS reaction following a formate-based path. The formulations of reaction rates based on this hypothesis have been validated multiple times with experimental data and are amongst the most popular in modelling of the reactors [62] [63].

In another type of kinetic model developed for methanol synthesis, certain variations of operating conditions influence active surface of the particles, which results in change of the number of oxygen vacancies at Zn-O-Cu interfaces. This was an improvement of a model proposed in former studies [64]. According to the model, depending on ratio of CO/CO_2 of mixture in contact with catalyst surface, the number of available active sites at the catalyst would change [65]. The authors report an improved description of the kinetic measurement over working methanol catalyst compared to a static kinetic model.

An extended microkinetic model based on DFT was proposed by Grabow and Mavrikakis, which included novel reaction intermediates and allowed new possible reaction by-products [66]. The proposed model included 49 elementary steps and no assumption on rate determining step. They estimated that about 2/3 of methanol is produced through CO_2 hydrogenation, however also other pathways were included, such as formation reaction of several by-products and intermediates. Another kinetic model based on a three-site adsorption n (Cu+1, Cu0 and ZnO) was proposed [67] [68], as an extension to previous research [69].

It is recommended for an interested reader to explore available review literature on kinetic models [52]. The only presented formulation of kinetics in this thesis is the most popular relation developed by Graaf [57] :

$$r_{CO\rightarrow CH_3OH} = \frac{k_1 K_{CO}[f_{CO} f_{H_2}^{3/2} - f_{CH_3OH}/(f_{H_2}^{1/2} K_1^{eq})]}{(1 + K_{CO} f_{CO} + K_{CO2} f_{CO2})[f_{H_2}^{1/2} + (K_{H_2O}/k_{H_2}^{1/2}) f_{H_2O}]} \quad \text{(VIII)}$$

$$r_{RWGS} = \frac{k_2 K_{CO_2}[f_{CO_2} f_{H_2} - f_{H_2O} f_{CO}/K_2^{eq}]}{(1 + K_{CO} f_{CO} + K_{CO2} f_{CO2})[f_{H_2}^{1/2} + (K_{H_2O}/k_{H_2}^{1/2}) f_{H_2O}]} \quad \text{(IX)}$$

$$r_{CO_2\rightarrow CH_3OH} = \frac{k_3 K_{CO_2}[f_{CO_2} f_{H_2}^{\frac{3}{2}} - f_{CH_3OH} f_{H_2O}/(f_{H_2}^{3/2} K_3^{eq})]}{(1 + K_{CO} f_{CO} + K_{CO2} f_{CO2})[f_{H_2}^{1/2} + (K_{H_2O}/k_{H_2}^{1/2}) f_{H_2O}]} \quad \text{(X)}$$

3 Research methods

The main purpose of this thesis was to create and validate a computational fluid dynamics (CFD) heat transfer model for the laboratory Power to methanol reactor, which was designed and built at Aalto University. Such a model enables the possibility to simulate and investigate the thermal behaviour of the reactor in transient operation, predicting the temperature distribution across its volume over time. The possibility to predict the temperature levels prior to the actual experiments with the chemical reactor setup is useful for experiment planning and ensuring the experimental setup remains in its safety margins all the time during its operation.

3.1 Experimental setup

The core part of the experimental setup is the methanol reactor. It is shown in Figure 7 in a disassembled state. It is a catalytic fixed bed reactor with direction of the fluid flow from top to bottom. Main dimensions of the reactor are presented in Tab 1. The inlet fluid in a steady state operation is a gaseous mixture of CO_2 and H_2 in the ratio of 1:3. The reactor's internal space is filled with a fixed bed made of particles of inert material and catalyst pellets. The catalyst pellets are fixed in the internal space of the reactor in a way to form a uniform layer in the shape of a cylindrical plug. Chemical composition of the catalyst is shown in Tab 2.

Figure 7: A methanol synthesis reactor in a disassembled state.

Tab 1: Main dimensions of the reactor

Volume	$0.57\ l$
Length	$500\ mm$
Nominal Flow rate	$500\frac{nl}{h}$
Reactor diameter	$38\ mm$
Oil jacket dimensions	$d_{oil\ min} = 50\ mm$ $d_{oil\ max} = 55\ mm$
Inert material	SiC particles

Tab 2: Chemical composition of catalyst

Al_2O_3	10.1 %
CuO	63.5 %
ZnO	24.7 %
MgO	1.3 %

The Power-to-X reactor setup was designed and built in Aalto University to research into how different operating conditions influence the composition of reaction products. The reactor's design and construction had been covered by another master's thesis prior to writing of this thesis [70]. These operating conditions include temperature and pressure inside the reactor, both inlet and outlet volumetric flow rates of the fluid, as well as heating and cooling rates through the oil jacket.

To achieve necessary data readings and control over operating conditions, the equipment is fitted with multiple sensors and actuators. Figure 8 shows the layout of the complete experimental setup with the reactor located in its central part.

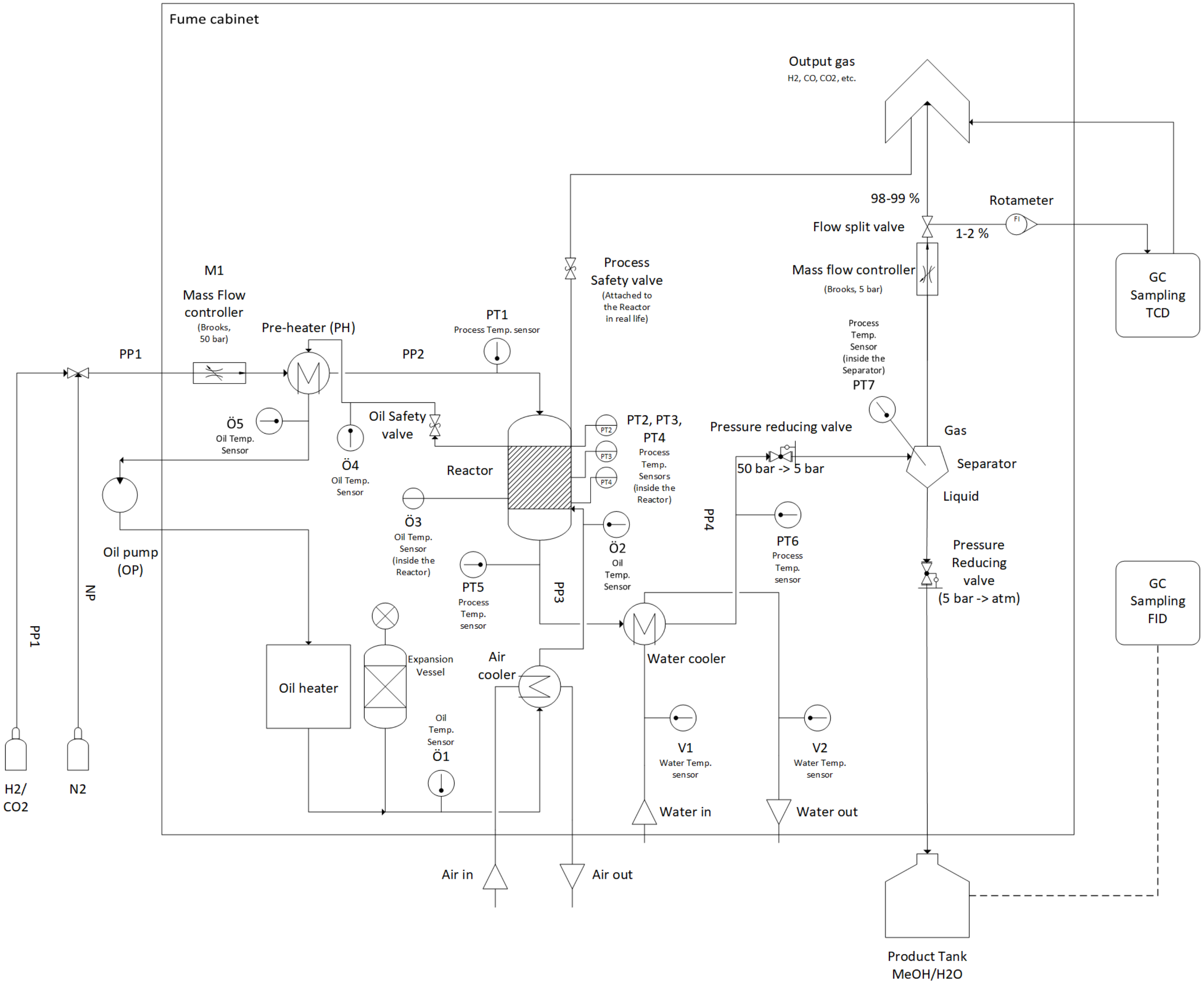

Figure 8: Layout of complete experimental setup with a Power to methanol reactor in its central part.

3.1.1 Process fluid system

The role of a process fluid system is to carry the stream of reactants to the reactor and carry the stream of products further, through subsequent components, such as a phase separator. The process fluid system has three states of operation:

1. Inlet valves are completely shut, there is no fluid flow.
2. The supply fluid is the inert N_2 gas.
3. The supply fluid is the mixture of CO_2 and H_2 with volume ratio 1:3.

N_2 is chemically inert against all other process fluid system elements in the operating conditions of the reactor. It is used as a process fluid in stages of start-up (heating up) and shut down (cooling down) of the experimental equipment. It is also necessary for safety reasons if any unexpected situation happens.

In the steady state operation, a reactant gas (CO_2 and H_2 mixture) flows out of a pressurised gas cylinder. Next, the gas flows through a first mass flow controller (MFC), which controls the volumetric flow rate and can be set to a desired value. Subsequently, the gas is heated by an oil-gas pre-heater and enters the reactor from the top.

The reactants flow through the reactor and partially react into products. The product gas stream contains H_2, CO_2, MeOH, H_2O, CO and an amount of other products, which are accounted as impurities. After exiting the reactor, the gas flows through a water-gas cooler, after which some of the stream components are expected to partially condensate: MeOH, H_2O and possibly other impurities.

The next step for the stream is to flow through a pressure-reducing valve into a separator tank where the liquid phase is separated from the gas phase. The liquid outlet located at the bottom of the tank leads to another pressure reducing valve which reduces the pressure of that stream to the atmospheric level, allowing the liquid phase of products to accumulate in the liquid tank. The other stream exiting the separator tank is a gas stream. It leads to a second MFC, after which the stream is directed to the exhaust channel.

3.1.2 Oil system

The role of the oil system is to control the temperature level of the reactor and incoming process fluid stream. The oil is *Shell Heat Transfer Oil S2*, which has its operating range between 0°C and 340°C. At first, the oil is heated by a resistance oil heater of a maximum power of 10kW. Although this value is significant, the heating power which effectively can be transferred to the reactor internal space is lower. This is due to relatively small area of oil jacket around the reactor, heat transfer between the reactor and the environment remaining in room temperature, and low temperature difference between reactor internals and heating oil due to a constraint for maximum oil temperature of 250°C because of limits of certain components in the oil system. Also, there are significant heat losses to the environment due to relatively small volume/area ratio of the reactor as well as piping.

Subsequently, the oil stream passes through an oil cooler, which is an oil-air heat exchanger with forced airflow. This oil cooler is used instead of the oil heater during its operation in high loads. This is required when the total system heat balance becomes positive and there arises the need for additional cooling instead of heating to stabilise the temperature.

Next, oil flows through an oil jacket of the reactor. The oil jacket is shorter than the inside space of the reactor, beginning with 60mm offsets from both ends of the reactor. During the operation, the oil flows in a counter-current manner in relation to the process fluid. After flowing through the reactor, the exiting oil stream is used to preheat incoming process fluid in the gas-oil preheater. The last element of the oil system is an oil pump, which controls oil flow rate through appropriate engine inverter setup.

3.1.3 Sensors

The experimental setup is equipped with different sensors both to ensure the necessary operating conditions and to gather results from experiments reported in this thesis. The key results of these experiments are the volumetric concentrations of product fluids outflowing from the reactor. These concentrations are necessary data to calculate fundamental indicators for any chemical reactor: reaction yield and selectivity.

The measurement of these product fluid compositions is performed with two gas chromatographs (GC): first one for analysis of liquid samples from the liquid product tank and the second one for gaseous phase analysis from the top of the separator tank.

Suitable operating conditions of the experimental setup are ensured with measurements pressure sensors, temperature sensors. There are 12 resistance temperature detectors (RTDs) of type *PT100*, which 3 of which are in the reactor to measure process fluid temperature, 4 are in different parts of the process fluid system (before and after the reactor), and 5 are assigned to oil system. These process fluid system RTDs are named *PT1, PT2, … , PT7*, while the oil system RTDs are named *O1*, *O2*, ... , *O5*. The sensors measuring the temperature inside the reactor are *PT2*, *PT3*, *PT4*, *O2*, *O3*, *O4*.

There are 3 thin-film-on-steel pressure transmitters. They are named *P1, P2, P3*. All of them measure the pressure inside the reactor.

The location of all reactor sensors is shown in Figure 9.

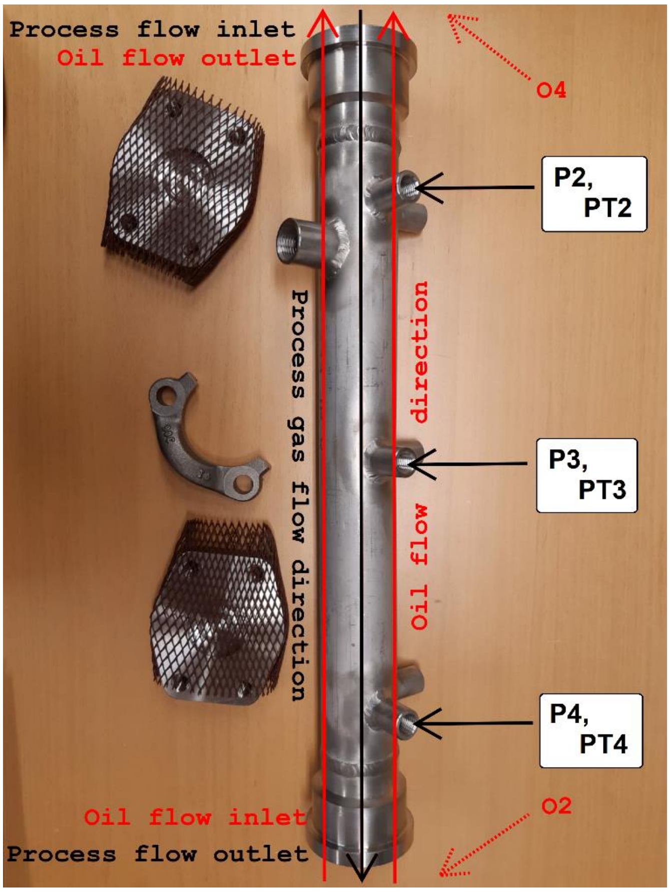

Figure 9: Location of the reactor sensors

3.1.4 Actuators

Actuators serve to setting desired operating conditions in the reactor. Setting the temperature is performed by turning a knob of the resistance oil heater to a desired value, with maximum power of the oil heater is 10kW.

In high reactor loads (close to its designed operating conditions), oil cooling is used instead of heating. Oil cooling is controlled by opening a pressurised air valve, which opens the airflow of a room temperature air into the oil cooler. The flow rate of the airflow is controlled with a knob.

Another parameter of reactor's operation is the flow rate of process fluid. This flow rate is adjustable by two MFCs, one of which is dedicated for the reactant gas inflowing to the reactor, while the second one controls the product fluid outflowing from the reactor. The MFCs are set to desired flow rate values with the common control panel. The presence of two units of MFCs is dictated by the quality of expected chemical reactions, as CO_2 hydrogenation reaction is a reaction with changing volume. This means that with the purpose of maintaining constant pressure in the reactor, inflow shall be different from outflow.

The next essential functionality in a laboratory scale chemical reactor is gas selection between process gas and inert gas. The gas selection valve is a manual valve with only two positions: either process gas or inert gas. This valve provides not only safe start up and shut down, but also the precise control of process gas injection timespan. The latter feature is useful in initial tests of the equipment and had a key role in performance of experiments reported in this thesis.

Finally yet importantly, there are two additional condition necessary to set the pressure in the reactor to a desired set point. The first condition is that pressure in the pressurised gas cylinders (both process gas and inert gas) is required to be higher than the pressure in the reactor. This pressure is controlled via manual reduction valves assembled on top of the gas cylinders. The second condition is that a manual pressure reducing valve between the reactor and the separator needs to be set to a set point between being open too much (pressure after the valve would be too high) and being completely closed, which would allow no fluid flow.

The photograph of the experimental equipment is presented in Figure 10. This photograph was taken in the stage of setting up the system, before glass wool thermal insulation was applied onto hot parts. The vertical columns located in the central part of the photograph are the separator tank and the reactor. The separator tank, on the left, is thinner and longer, while the reactor, on the right, has lower length-to-width ratio.

Figure 10: Experimental equipment without insulation. The reactor and separator vessels are seen in the middle.

3.2 CFD model for heat transfer

Another method used in this thesis is the simulation of thermal conditions in the methanol reactor with a CFD model. The model was developed specifically as an aid in experimental research on this particular power to methanol reactor. The main purpose of simulating heat transfer is to provide a wide overview of the thermal conditions in the reactor, which cannot be determined from the experiments alone. Such a model allows to recreate the experiments using simulations with specified accuracy, thus providing the temperature results for every part of the reactor. These results present a bigger picture in contrast to a limited number of sensor measurements from experiments. Another case for aiding experimental research with CFD simulations is the possibility to simulate certain scenarios in advance of performing the experiments. Such simulations enable early prediction of results, parallel to evaluation of safety, which allows timesaving and planning further experiments with higher precision. Results of these simulations are temperature values in all areas of the reactor, available in intervals of 1 sec.

3.2.1 Geometry and mesh

In CFD modelling, the first step of creating a new model is forming its geometry, with specified simplifications. For the model introduced in this thesis, such simplifications include the representation of the whole reactor component as a shape made of cylindrical shapes. Figure 11a illustrates complete volume of the reactor model. The oil jacket is represented as an orange tubular shape, with the direction of oil flow signalized by white arrows. The reactor internals, which are surrounded by the oil jacket, are marked with purple colour.

The presence of the steel walls of the reactor structure was omitted during model development, meaning that there is no physical mass nor heat capacity of the steel walls included into the model. Although the reactor is surrounded with a layer of glass wool in the experimental setup, the presence of such wool was also omitted, meaning that there is no mass nor heat capacity related to it neither. The external surfaces of the reactor are in direct contact with the environment, which is at room temperature. Although both structural steel and isolating wool were not included into the model, their effects related to heat conductivity across the material interfaces are included into the physics, due to heat transfer coefficient calibration described in chapter 3.3.1.

The internal volume of the reactor, which is marked with purple colour, is a closed space, which is filled with fixed bed consisting of SiC particles and a layer of catalyst particles. During reactor's operation, the process fluid is also moving through that space. Because of complexity of such fixed bed space, another geometric simplification was implemented. The internal reactor volume was divided into two sub-volumes, which can be seen in Figure 11b. The first sub-volume is of cylindrical shape (blue colour) and represents the fluid moving through the reactor, while the second sub-volume is of tubular shape (green colour) and portrays the solid mass of fixed bed particles. This particular simplification allowed to easily separate the physical parameters of fixed bed from such parameters of moving fluid, while also allowing these media to have different temperature values across all simulations. These kinds of models, where bed particles are detached from the fluid moving across the bed are called heterogeneous models. The modelled space is 2D axisymmetric, based on geometric properties on the infinitesimal axial section shown in red colour in Figure 11.

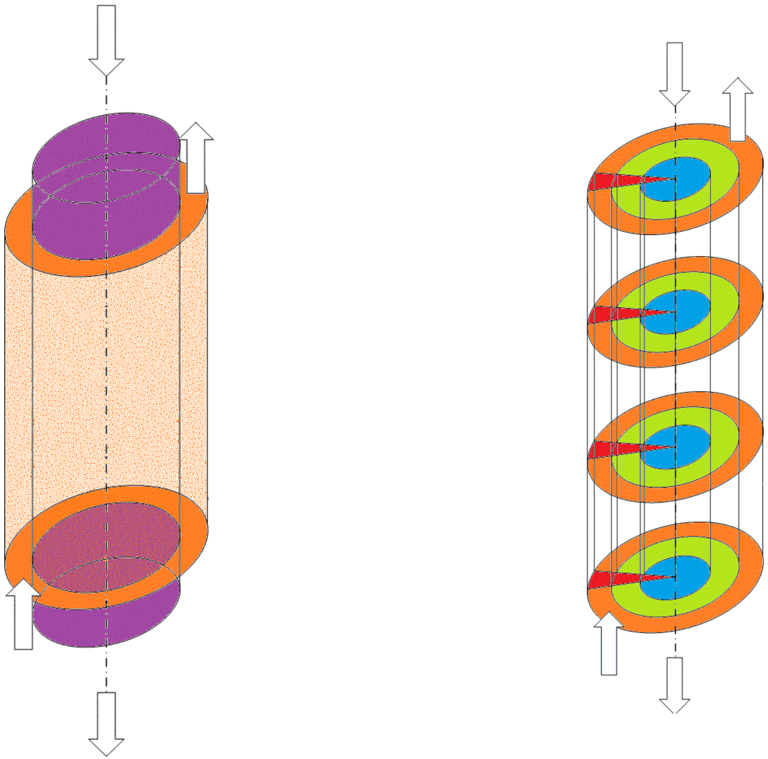

Figure 11a

Figure 11b

Figure 11: Representation of the reactor volume by a CFD model.

After defining geometry, the model was divided into a mesh, which is shown in Figure 12. In the model visualization, length of the reactor is represented by a vertical axis. The second dimension is radius with relation to the axis of the model. The space has been divided into 300 elements in total, which are 100 elements lengthwise and 3 elements radius wise. In the bottom and central part of the reactor, starting from the axis, the first finite element layer represents fluid inside the reactor, the next finite volume layer stands for solid and the last finite volume layer refers to oil. Such a space discretization method means that in each of the mediums (fluid/solid/oil) the temperature is uniform in the radius direction, because there is only one element layer per each medium. Therefore, there is no radial temperature distribution present inside these separate layers and the only radial heat transfer is through interfaces with other mediums. Additionally, all the movement of both oil and process fluid is reduced to one-dimensional case with only vertical flow allowed.

In the top part of the mesh shown in Figure 12, there is a distinctive dark area, which depicts the top part of the reactor. In this part, there is no fixed bed any more, but rather the space is completely filled by fluid. This space was left without fixed bed fill intentionally with the aim to compensate thermal expansion.

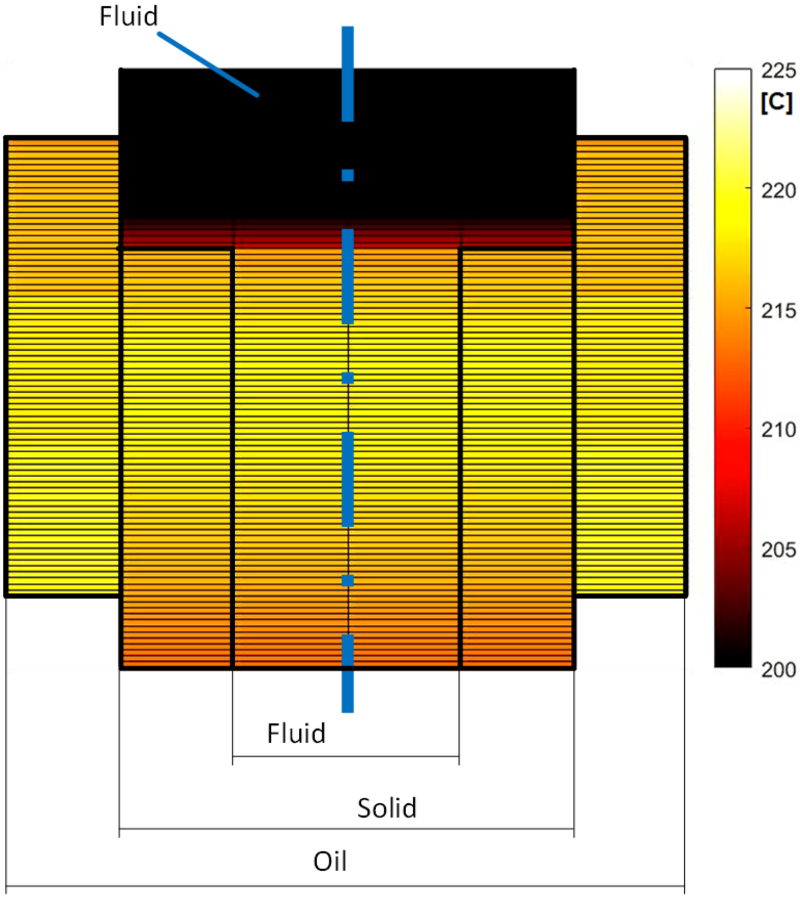

Figure 12: Mesh of the 2D axisymmetric CFD model of the reactor.

The next simplification relates to unification of fixed bed properties. The properties of the whole fixed bed were unified to parameters of SiC fixed bed, which means there is no distinction in thermal parameters between the 7 cm thick catalyst layer and the supporting inner material.

3.2.2 Physics simplifications

Further physical simplification of the model is the assumption of constant properties of all the materials, independent of temperature and process fluid composition. These constant properties include material density and heat conductivity. Both the fluid inside the reactor and the oil in the oil jacket have the velocities explicitly specified and set at constant values. Due to these modelling assumptions, the outlet flow rate of the process fluid has the same value as the inlet flow rate in every simulation.

Due to the fluid movement being reduced to 1D case with only one element of each medium radius-wise, several fluid mechanics phenomena, such as turbulence, natural convection or law of the wall, are not taken into account in the modelling physics. Furthermore, heat transfer by radiation is also not included. The only two mechanisms present in the model governing heat transfer in process fluid and oil are heat diffusion and forced convection, which are described with a convection-diffusion equation:

$$\rho_f C_{p_f} \frac{\partial T}{\partial t} + V_f \rho_f C_p \nabla T = \nabla\left(k_f \nabla T\right) + \dot{q} \tag{9}$$

where:

ρ_f – fluid density $\left[\frac{kg}{m^3}\right]$, C_{p_f} – fluid heat capacity $\left[\frac{J}{kgK}\right]$,
T – fluid temperature $[K]$, V_f – fluid velocity $\left[\frac{m}{s}\right]$,
k_f – fluid heat conductivity coefficient $\left[\frac{W}{mK}\right]$, $\dot{q}$ – external heat $\left[\frac{W}{m^3}\right]$.

Heat transfer between the fluid and any other medium is assigned to the term of external heat $\dot{q}$, which is quantified as:

$$\dot{q} = \alpha(T_1 - T_2) \tag{10}$$

where:

α – heat transfer film coefficient across the interface of adjacent media $\left[\frac{W}{m^2K}\right]$,
T_1, T_2 – temperatures of adjacent media $[K]$.

Inside the solid medium, representing reactor’s fixed bed in the model, the heat transfer physics is reduced further and its only mechanism is diffusion. Therefore, the heat transfer in solid follows the law of heat conduction (Fourier’s Law):

$$\rho_s C_{p_s} \frac{\partial T}{\partial t} = \nabla(k_s \nabla T) + \dot{q} \tag{11}$$

where:

ρ_s – solid density $\left[\frac{kg}{m^3}\right]$, C_{p_s} – solid heat capacity $\left[\frac{J}{kgK}\right]$, T – solid temperature $[K]$, k_s – fixed bed heat conductivity coefficient $\left[\frac{W}{mK}\right]$, $\dot{q}$ – external heat $\left[\frac{W}{m^3}\right]$.

The parameter k_s refers to the conductivity coefficient of fixed bed of SiC particles.

3.2.3 Numerical method

The continuum discretization method of choice for the model is FVM. FVM is an alternative of Finite Difference Method (FDM), which utilizes discretization of space into volumes, allowing to take into account physical conservation laws for each enclosed finite volume. These conservation laws include conservation of mass and energy, which are particularly important in energy applications related components. Euler first order implicit method was chosen to solve the resulting set of ordinary difference equation. The simulation time step was set to a length of 1 sec. For convection modelling, the upwind differencing scheme was selected because of its simplicity in implementation. The whole numerical model was developed in MATLAB and the solver was chosen automatically based on *mldivide* function for solving linear system of equations.

3.3 Performed experiments and simulations

3.3.1 Calibration of coefficients of heat transfer

One of the necessary steps in creating a useful heat transfer FVM model is determination of heat transfer coefficients between adjacent finite volumes. These coefficients can be estimated based on dimensionless equations from literature. In case of complex geometries, which are simplified for the sake of obtaining a simple model, it is, however, likely for these estimations not to achieve desired level of accuracy. In these cases, estimating the heat transfer coefficients based on experimental results can lead to higher modelling precision. In literature, there are several examples of evaluating experimental heat transfer coefficients of fixed bed reactors [71] [72] [73], including experiments designed especially for identification of these coefficients [74] [75] [76] [77] .

In the model presented in this thesis, the heat transfer coefficients needed to be estimated across five interfaces:

c_{fb} – interface between fluid and bed,
c_{bo} – interface between bed (solid) and oil,
c_{bet} – interface between bed and environment (at the top),
c_{beb} – interface between bed and environment (at the bottom),
c_{oe} – interface between oil and environment.

These interfaces are marked with green lines in Figure 13 and marked with titles of corresponding coefficients.

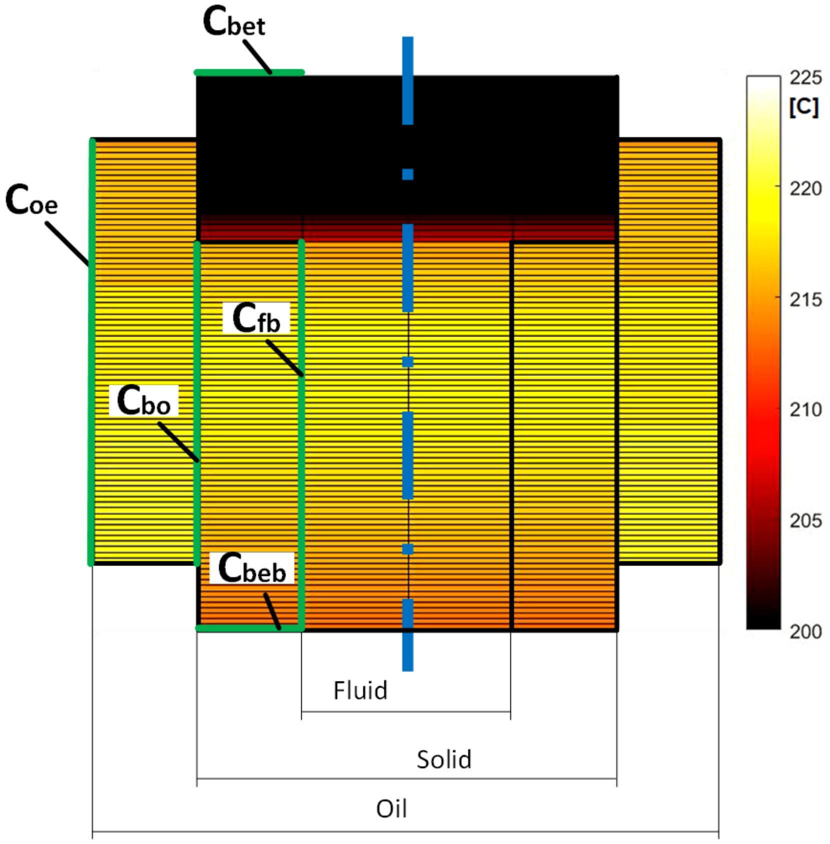

Figure 13: Heat transfer coefficients and their corresponding material interfaces in the CFD model.

All of the coefficients presented above refer to complex heat transfer geometries, although in the model they are represented as simple 2D boundaries. For instance, c_{bo} is the assumed film coefficient between bulk solid mass of fixed bed and oil, while in reality it represents the heat transfer between porous bed and the stream of oil across thick metal reactor wall, with two material interfaces on both sides. As a following example, c_{fb} represents heat transfer between bulk solid mass of uniform fixed bed material and uniform process fluid stream. The coefficient c_{fb} is derived from previously reported simplifications of physics and relates to simple heat conduction between bed and oil. On the contrary, in reality the fluid is a mixture of different compounds, the bed is composed of SiC particles and catalyst pellets of different porosity, and the physics is governed by complex phenomena, such as turbulence.

There is no possibility to measure the values of these coefficients separately in isolated conditions. The change of one of such coefficients affects the dynamics of heat transfer, influencing the whole model. However, it is possible to numerically estimate such heat transfer coefficients by fitting the simulated temperature curves with minimum possible error to the experimental temperature curves obtained from measurements of installed sensors.

One such a method is non-linear regression. It allows to find the coefficients of a non-linear function, which satisfy the condition of minimising the least-square error between given the function results and reference data:

$$\underset{\boldsymbol{c}}{\boldsymbol{min}} \, \|\boldsymbol{F}(\boldsymbol{c}) - \boldsymbol{ydata}\|^2 = \underset{\boldsymbol{c}}{\boldsymbol{min}} \sum_{\boldsymbol{i}} (\boldsymbol{F}(\boldsymbol{c}) - \boldsymbol{ydata_i})^2 \tag{12}$$

where $\boldsymbol{c}$ are wanted coefficients, $\boldsymbol{ydata}$ are the reference experimental results, and $\boldsymbol{F}(\boldsymbol{x})$ are simulation results from the model.

The reference $\boldsymbol{ydata}$ was extracted from one of the experiments, which included dynamic heating and cooling of the reactor by the oil flowing through oil jacket. Such data was specifically chosen to for the coefficient calibration to capture the dynamic relation between measured values from different sensors. The steep changes in oil temperature were achieved through manipulating the oil cooling through switching it on and off. Through this experiment, the reactor was not operational, which means there was no chemical reaction proceeding, as the only fluid flowing through the reactor was N_2. This allowed to ensure the independence of results from the chemical reaction conditions. With the aim to keep the clarity of the figures, the temperature curves from this experiment were divided into 6 pieces of a unified length of 2200 seconds. The curves are presented in Figures 14-17.

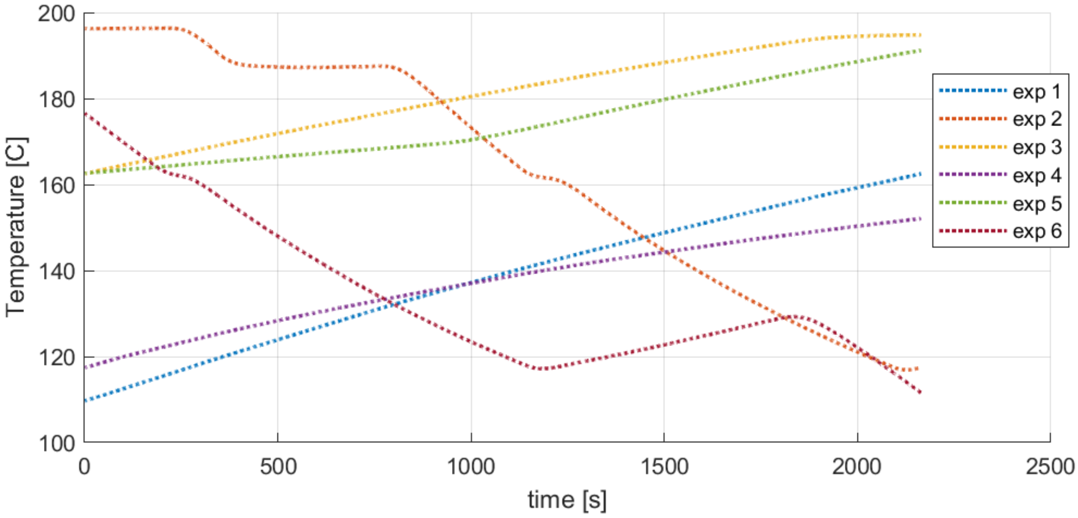

Figure 14: Temperature measurements at the catalyst layer (*PT3*) - dynamic heating and cooling.

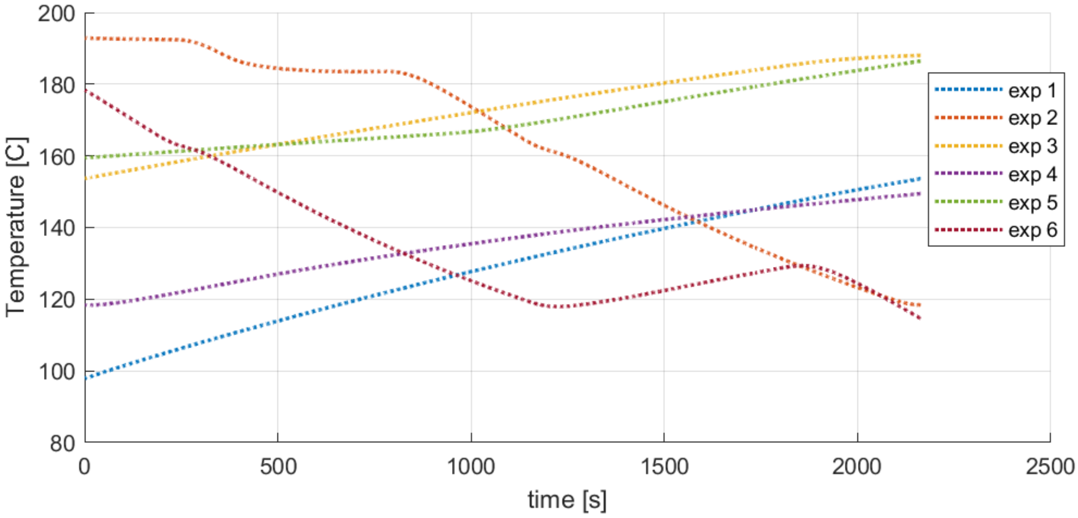

Figure 15: Temperature measurements at the bottom part of the reactor (*PT4*) - dynamic heating and cooling.

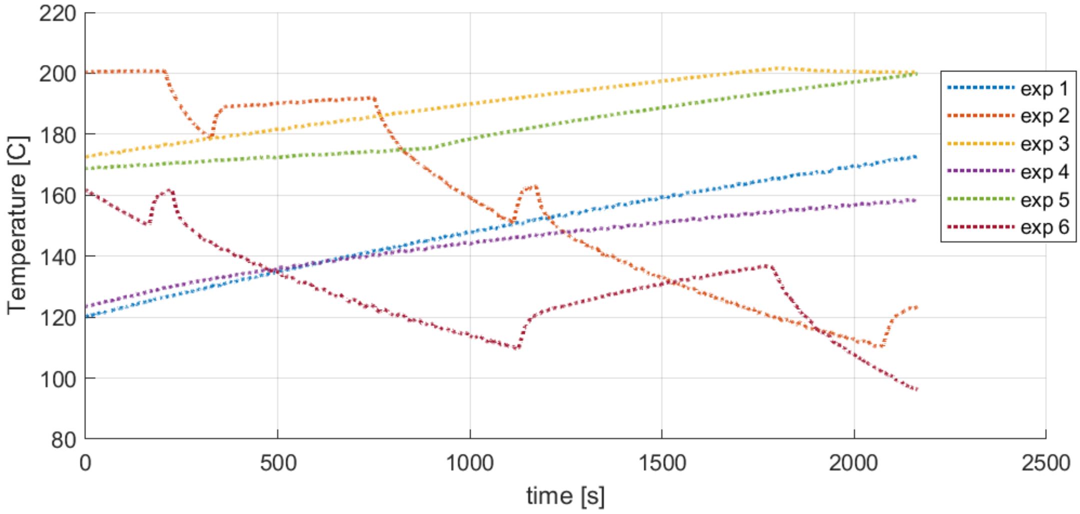

Figure 16: Temperature measurements at the oil outlet from the reactor (*O4*) - dynamic heating and cooling.

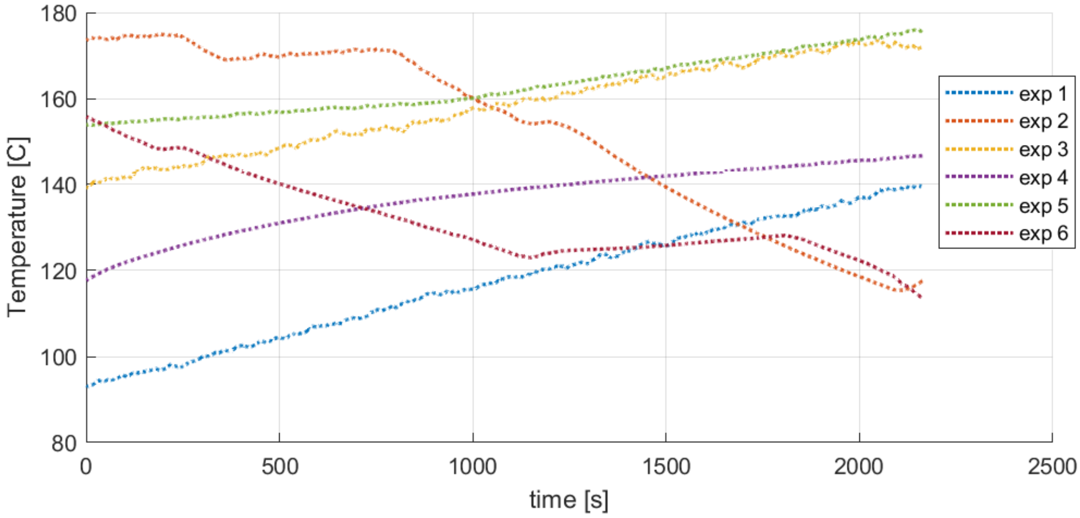

Figure 17: Temperature measurements at the top part of the reactor (*PT2*) - dynamic heating and cooling.

Non-linear regression was performed with MATLAB function *lsqcurvefit*. The acceptable level of simulation error using the calibrated model is in the order of 10°C. If the error is within that range, the model is accurate enough to be an aid in answering the stated research questions.

3.3.2 Experiments in partial load of the reactor

After calibrating the model with the data originated from, the next step was to run the reactor with a chemical reaction proceeding in partial load. The reason for not performing it on full load was safety concern about possible overheating of the catalyst layer. Process temperature conditions inside the reactor have been reduced in relation to the nominal ones, being as following:

$$p = 50\ bar, \qquad T = 215\ °C, \qquad v_{reactants} = 500\,\frac{Nl}{h}$$

In total, three experiments were performed. Prior to the beginning of each experiment, the reactor was required to achieve steady-state conditions in terms of pressure, temperature and volumetric flow of inert N_2 gas through its bed. In these conditions, the reactant injection began with gas selection valve switch from ”inert gas” position to ”process gas”. After a specified time span of the experiment, the gas selection valve was switched back to its primary position. The experiments were all performed in similar conditions, with the varying parameter being process gas injection timespan. The aim of varying this timespan was to capture differences in reaction dynamics between shorter and longer reaction timespans, as well as to investigate the time required for the reactor to achieve steady state conditions. Pressure data was also recorded during each of experiments, allowing to capture any trends in pressure change due to chemical reactions occurring. This is due to the fact that both MFCs installed at the inlet and at the outlet of the system were set to allow for the same volumetric flow rates.

3.3.3 Recreation of experiments with simulations

The model presented in this thesis does not include any chemical reaction kinetics. However, from the perspective of expected simulation results, the only necessary information is the rate of heat generation (or heat absorption) in the volume of the catalyst. Such heat generation can, with further modelling simplifications, be assumed to take place uniformly in the catalyst layer of reactor’s fixed bed. Under that assumption, it is possible to compare experimental results of temperature inside the reactor with the results of simulations. The estimation of heat generation during unsteady reactor operation can be difficult and subjected to additional errors, therefore all the estimations of heat generation with the model introduced in this thesis were performed referring the steady-state reaction conditions.

Two sources of information were used to estimate the total amount of heat generated. The first one was the rate of pressure drop in the reactor during steady-state chemical reaction, the trend of which was estimated from results presented further in chapter 4.2. The second source of that information was the temperature measurement from the longest one of three experiments, where the steady state of reaction was achieved. By comparing this value with the corresponding steady state value from the simulation, it was possible to estimate the rate of heat generation, at which the simulated result would be the closest possible to the experimental one. All reaction enthalpy values in this thesis were estimated using Kirchhoff's Law based on reference values of standard enthalpies of reaction and enthalpy values at specific operating conditions found in the thermodynamic tables.

3.3.4 Uncertainties in experimental and simulation results

Measurements performed inside the reactor are subject to measurement uncertainties, specified by digital sensor suppliers. For the temperature sensors, Nokeval PT2T, the total uncertainty is 0.05% of full scale (700°C range) together with 0.05% linearity error of the measured value. For the pressure sensors, Trafag EXNT100.0A, the uncertainty is 0.5% of full scale (100 bar range). Therefore, total measurement uncertainties of pressure and temperature measurements presented in this thesis are the following:

$$\delta T = \frac{0.05}{100} * 700\ ^{\circ}\mathrm{C} + \frac{0.05}{100} * 200\ ^{\circ}\mathrm{C} = 0.45\ ^{\circ}\mathrm{C} \tag{13}$$

$$\delta p = \frac{0.5}{100} * 100\ \mathrm{bar} = 0.5\ \mathrm{bar} \tag{14}$$

The numerical model has been calibrated using experimental values, which are subject to such uncertainties. By result, the accuracy of resulting heat transfer coefficients is also affected. It is difficult to quantify the exact uncertainty in the coefficient themselves, because the model is a complex non-linear function of these coefficients. A quantification of influence of such uncertainties would require conducting a proper sensitivity analysis of the model, and it was outside of the scope of this thesis.

Another source of uncertainty in temperature measurement is the presence of hot and cold spots in the reactor's fixed bed, where the measured values can differ greatly within short distance apart. When it comes to modelling results, other sources of uncertainties are also present. These include modelling simplifications, including geometry, physics, discretization and mathematical solver errors.

4 Results

4.1 Calibration of coefficients of heat transfer

The multiple regression curve fitting process outlined in 3.3.1 brought the results in the form of the following coefficients of heat transfer (note: in the numerical model, they appear with negative units):

$c_{fb} = 100\ \frac{W}{K}$ $\quad c_{bo} = 0.0234\ \frac{W}{K}$ $\quad c_{bet} = 0.1032\ \frac{W}{K}$

$c_{beb} = 0.03255\ \frac{W}{K}$ $\quad c_{oe} = 0.008532\ \frac{W}{K}$

These coefficients refer to certain interfaces in the model introduced in this thesis. They are represented in $\left[\frac{W}{K}\right]$ units instead of being converted into $\left[\frac{W}{m^2K}\right]$ units. This is due of the fact that they refer to particular finite volume interfaces, which are specific for this CFD model. These coefficients take into account all the assumptions and geometry simplifications of the model mentioned previously. Consequently, they should not be compared to reference values originated from literature.

4 of 5 obtained coefficients are in the anticipated range $\left[\frac{0.1\ W}{K}\right]$, whereas c_{fb} reached its upper boundary limit of $100\frac{W}{K}$. Considering large surface area of fixed bed, it is technically possible that without the upper boundary condition the regression model would find even higher c_{fb} coefficient value, which would result in more precise simulation result. However, with the value of this order, the heat transfer between fluid and bed is nearly instantaneous. Further increase in the upper boundary condition would not have any significance on the results, while it could prolong calculation times and lower precision of the regression model in relation to other coefficients.

The results of model calibration using derived coefficients are presented in Figures 18-21. The graphs show both experimental and simulated temperature values at different sensor locations: *PT3*, *PT2*, *PT4*, and *O4*. Experiments are represented by dotted lines, while simulations are shown in solid lines. Different colours illustrate various experimental pieces of data gathered from the experiments, which the curve fitting process was based on.

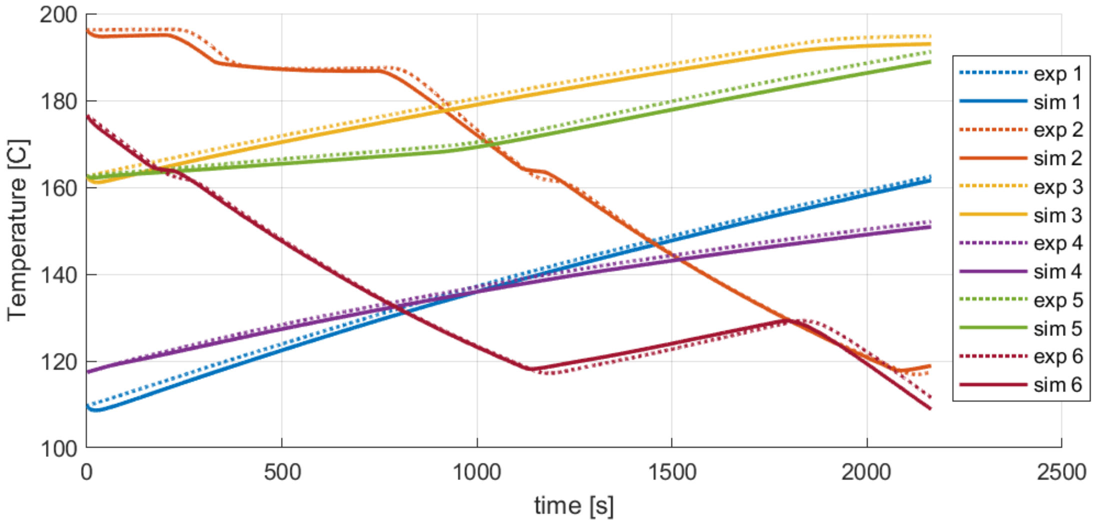

Figure 18: Temperature values of curve fitting data at *PT3* sensor (reactor internals at catalyst layer) - experiments (dotted lines) and simulations (solid lines).

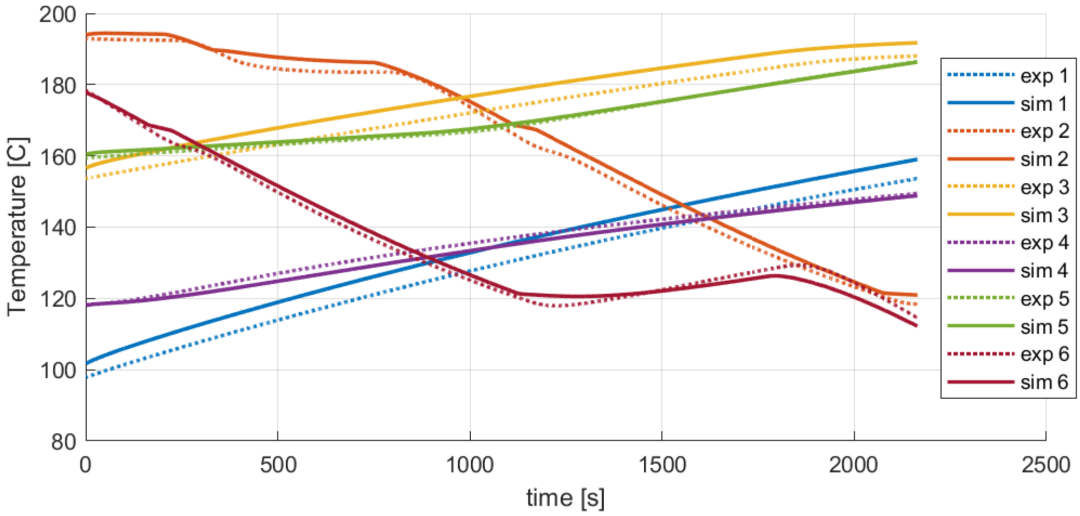

Figure 19: Temperature values of curve fitting data at *PT4* sensor (reactor internals at the bottom) - experiments (dotted lines) and simulations (solid lines).

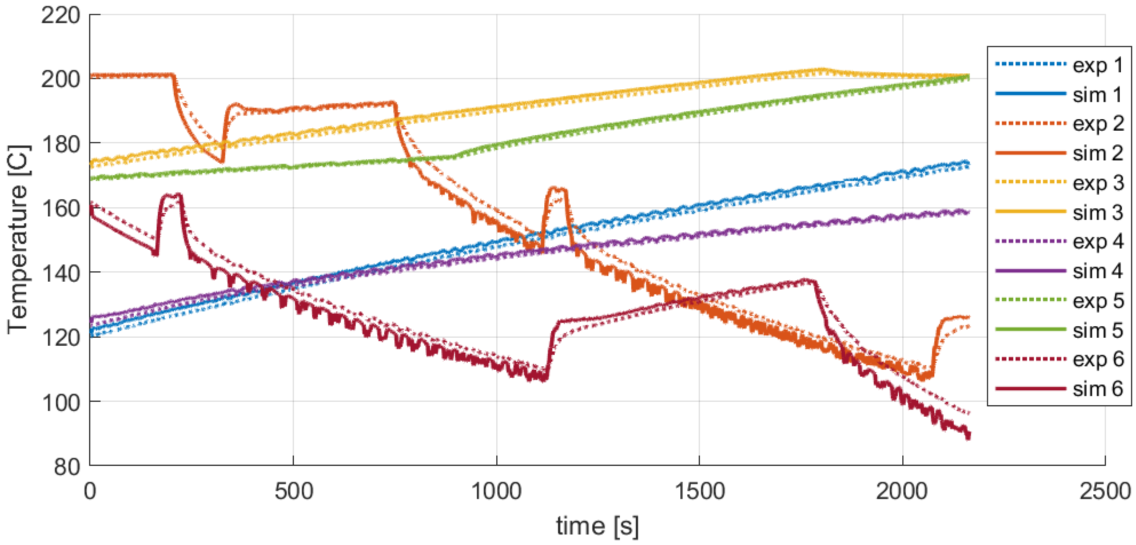

Figure 20: Temperature values of curve fitting data at *O4* sensor (oil outlet at the top) - experiments (dotted lines) and simulations (solid lines).

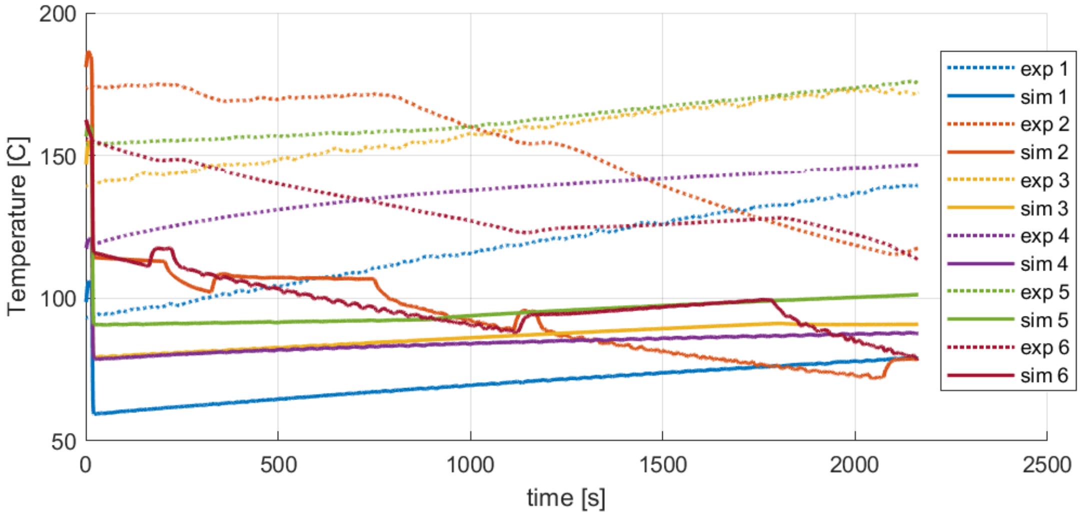

Figure 21: Temperature values of curve fitting data at *PT2* sensor (reactor internals at the top) - experiments (dotted lines) and simulations (solid lines).

Simulation outcomes shown in Figures 18-20 reproduce the results of dynamic experiments with useful level of accuracy, in terms of both shape and the order of errors. These errors do not exceed 5°C in Figure 18 and 10°C in Figures 19,20, which means that the necessary level of simulation precision has been reached at the measurement points of *PT3*, *PT4* and *O4*, that allows to evaluate future experiment plans and safety of reactor operation. This order of error is acceptable from the perspective of answering the research questions, while taking into account the experimental accuracy of the setup.

In Figure 20, there are visible oscillations of simulated oil outlet temperature in some of the curves, happening typically at lower temperatures. These oil oscillations are the consequence of temperature oscillations of the oil inflowing to the reactor. The origin of the oscillations are oil vibrations in the oil system, which cause time differences in heat transfer intensity at the oil heater. The possible reason for the model not dampening these oscillations to the necessary extent is the model simplification of not taking into account physical existence of steel oil jacket walls, which would help transferring heat lengthwise, smoothing out the oil outlet temperature.

Simulation results presented in Figure 21, however, are not a valuable reproduction of the experimental data, as the order of error exceeds 50°C and the shape of the curves is by no means similar. Thus, the temperature of *PT2* measurement point cannot be evaluated using the reported model. The data mismatch at Figure 21 showing *PT2* sensor is most likely caused by the fact that this sensor is in the upper part of the reactor, above the level of fixed bed. Such position implies that in direct proximity of the sensor there is only fluid, which makes the sensor highly susceptible to various fluid-related phenomena causing unstable temperature reading. These phenomena include turbulence, natural convection and wall effects, which highly influence heat transfer coefficient between the fluid and the sensor. The consecutive reason for the error of *PT2* data is the modelling method.

Although the model is precise enough to represent the temperature in the fixed bed area, its assumptions and simplifications limit its use so that it cannot represent well the behaviour of gaseous volume in the top of reactor. Specifically, the mesh of the model is too coarse and the time step of 1*s* is too short to process the aforementioned phenomena typical for fluids. Another limiting factor is that the velocity is assumed as explicitly known, steady, and radially uniform in the whole volume of the reactor. However, these issues are not disqualifying the validity of the whole model to plan experiments and access safety of operation, as the empty reactor space in its top part is not an expected area of high thermal loads.

4.2 Reactor operation in partial load

Figures 22-24 illustrate three temperature readings during experiments performed in mild conditions of the experimental setup. Two black vertical lines mark the beginning and the end of process gas injections to the system. Figure 22 shows the result of operation through experiment a) lasting

3 min 30 s. Figure 22 shows the result of operation through experiment b) lasting 10 min. Figure 24 shows the result of operation through experiment c) lasting 23 min 26 s. The X-axes of Figures 22-24 represent real time of the experiments and are in different scales in each of the figures.

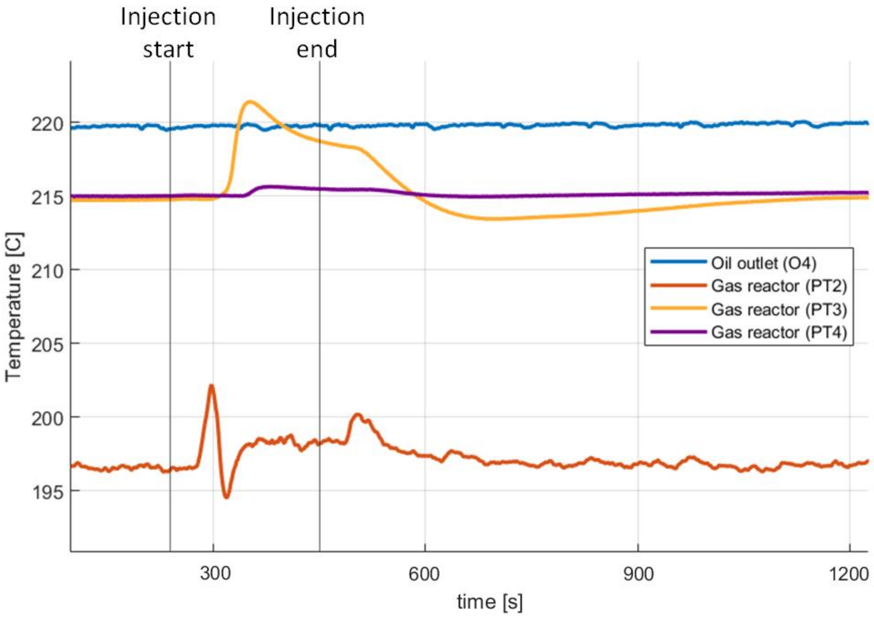

Figure 22: Temperature values during experiment a). Vertical lines mark the beginning and the end of process gas injection.

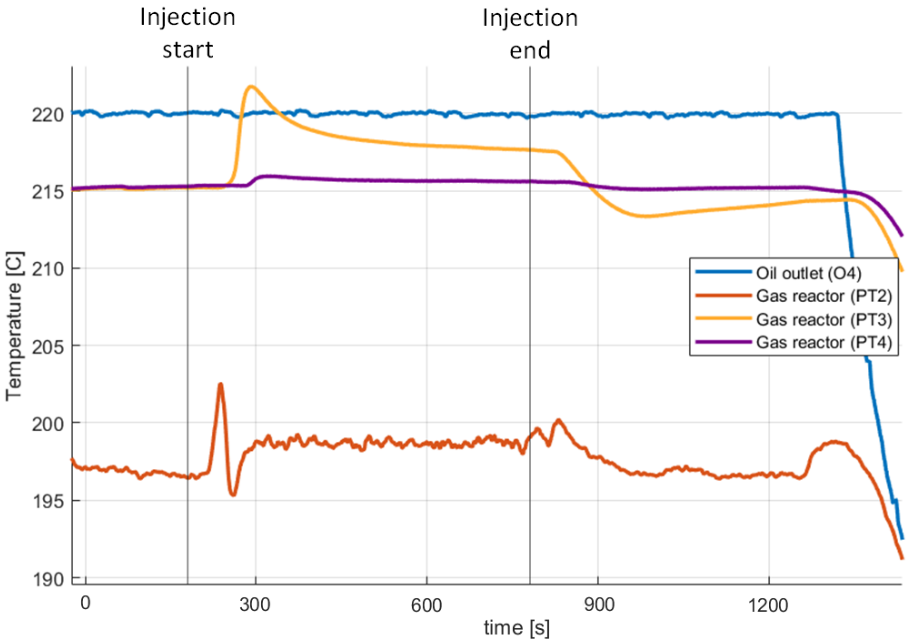

Figure 23: Temperature values during experiment b). Vertical lines mark the beginning and the end of process gas injection.

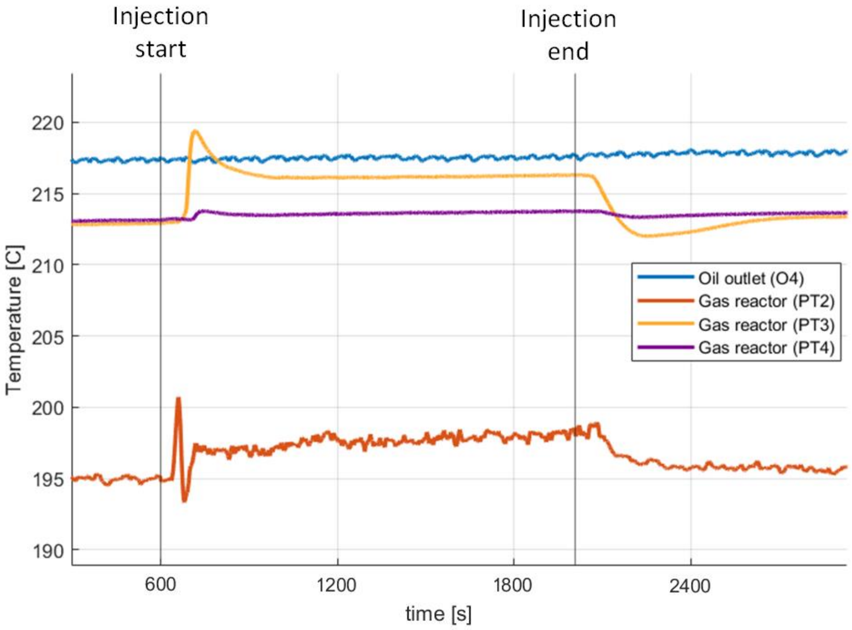

Figure 24: Temperature values during experiment c). Vertical lines mark the beginning and the end of process gas injection.

In all cases a), b), and c), the rise of temperature in the catalyst layer (*PT3*) can only be noticed after approximately 1 min from the beginning of reactants injection. This period of 1 min is the time, which is required for the process gas to be transported through piping to the catalyst layer of the reactor. Only after this time, the reaction begins to take place.

Initially, the temperature rises rapidly. This is due to introduction of process gas to fresh catalyst with plenty of unoccupied catalyst sites, where the reactants easily adsorb and react, releasing energy in the form of heat. Subsequently, the temperature peak is reached soon after and a steady decline takes place, having a shape of an asymptotic curve. This temperature decrease, together with expected eventual temperature stabilisation are results of reaction kinetics reaching a balance between new reactant molecules being adsorbed to the catalyst sites and product molecules freeing the used catalyst sites. Such balance manifests itself in (*PT3*) temperature stabilisation on lower level than its peak value. This can be observed in Figure 24 showing experiment c), while in Figures 22,23 illustrating experiments a) and b) the balance has not yet been reached because of reactants injection interruptions. It is expected that if these injections were longer in a) and b), the temperature values of the catalyst layer (*PT3*) would also eventually reach a steady state.

In all cases a), b), and c), approximately 1 min after the end of process gas injection, the temperature at sensor (*PT3*) begins to decline sharply. The reaction kinetics balance of adsorption and desorption is violated with the concentration of reactants not sufficient to match the intensity of desorption with intensity of adsorption. The rate of chemical reaction drops and *PT3* temperature diminishes significantly further than what would be expected from the material simply cooling off. The shape of the declining curve is not exponential with an asymptote towards the initial temperature before the reaction. Instead, the curve dips to values below that level, after which it slowly comes back to the steady state at the original value of *PT3* temperature. This dip below the primary temperature value is an indication of heat absorption, meaning the dominance of an endothermic reaction step, such as product desorption, in the reactor shutdown stage.

In all experiments a), b), and c), the shapes of the *PT3* temperature curves after the end of reactants injection are notably similar. The timespan of negative temperature values, in relation to primary temperature at steady state, is approximately 10 min in each of the cases, indicating similar shutdown conditions in the reactor regardless of operational timespan.

PT4 temperature readings, which refer to the reactor bed area at the bottom of the reactor, show similarities in shape to *PT3* readings, however they have notably lower magnitude and typical dilution of shape over time. These result differences between *PT3* and *PT4* portrait typical effect of heat diffusion and advection through the internal reactor volume. On another hand, *PT2* values, which refer to the empty reactor area at the top, do not follow the same regime. Heat diffusion-advection effects, which were seen previously in *PT4* readings, are, as expected, notably less influential in *PT2* results due to the upstream direction from the catalyst layer, which is a heat source during the reaction. Another reason is that the heat conduction coefficients of gases are lower than the same coefficients of solid bed.

The temperature spikes at *PT2* sensor location in initial stages of each of the experiments a), b), and c) are believed to be caused by the dynamics of heat transfer between process fluids and piping. Overall, *PT2* readings are expected to be strongly affected by the temperature and velocity of gases incoming into the reactor and can be treated as an indication of inlet gas conditions. *O4* sensor readings, which indicate oil outlet temperature, do not show any significant difference throughout any of the experiments, meaning that this temperature remains unaffected by reactor operation in mild conditions.

Figure 25 shows the relation of reactor pressure (*P2*) and temperature of the catalyst layer (*PT3*) during experiment b). Two black vertical lines mark the beginning and the end of process gas injection to the system.

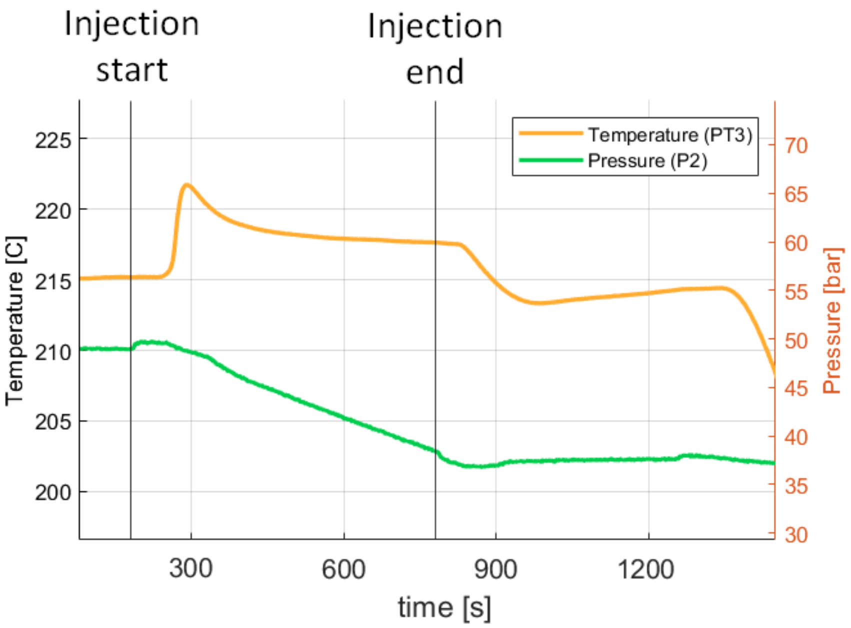

Figure 25: Reactor pressure and temperature of the catalyst layer during experiment b).

The pressure decline observed in the graph is fully attributed to the chemical reaction with decreasing volume. This is because mass flow controllers controlling both inlet and outlet flow rates were set to keep the pressure steady prior to the reactants injection, which excludes the influence of any leaks on such a pressure difference. Instantly after switching the inlet gas to reactants, pressure slightly rises, which is most likely the effect of mass flow controller transitioning its operation between inert gases and reactants. Subsequently, when the reaction starts occurring about 1 min later, the pressure begins to diminish over time.

After approximately 4 min from the beginning of the reactants injection, the rate of pressure decrease reaches steady state and the linear trend in relation to time can be noticed. This trend is marked with a brown line in Figure 26.

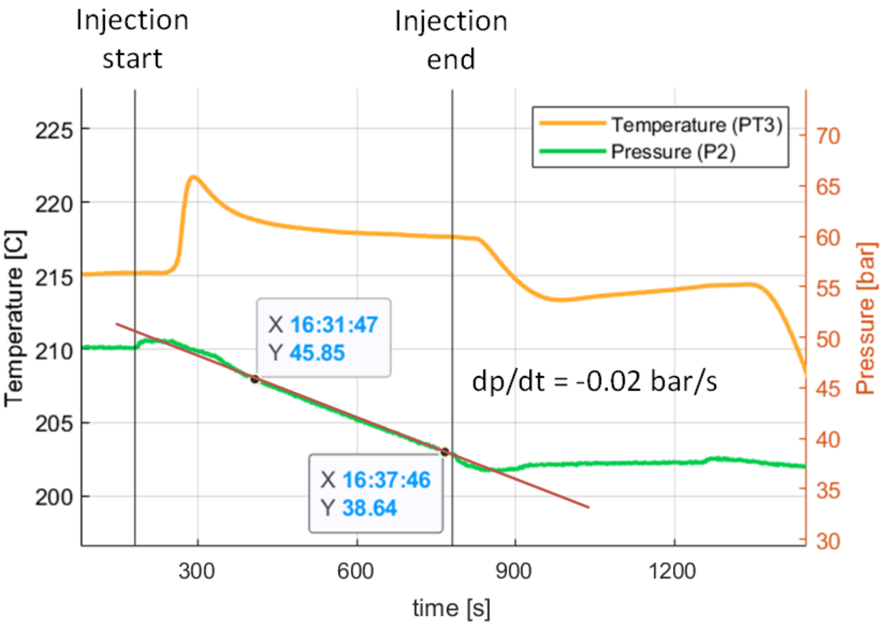

Figure 26: Steady state trend of pressure decrease during experiment b).

Inclination of the trend line denotes pressure decrease rate of $p_{decrease} = -0.02\frac{bar}{s}$ during steady state reactor operation in mild conditions. With this value, it is possible to estimate the number of CO_2 molecules, which underwent reaction, using the following formulas:

Reactor internal void space volume available for fluid:

$$vol_{fluid} \approx 3 * 10^{-4}\,\frac{Nm^3}{bar}$$

Amount of moles occupying volume of compressed gas as a function of pressure to facilitate calculations below:

$$vol_m = \frac{1}{22.4 \frac{l * bar}{mol}} * \frac{10^3 l}{m^3} = 44.643 \ \frac{mol}{m^3 * bar}$$

Volume decrease rate during steady state reaction in mild conditions:

$$v_{decrease} = vol_{fluid} * \ p_{decrease} = 3 * 10^{-4} \frac{Nm^3}{bar} * (-0.02) \frac{bar}{s} = \\ = \ 5.968 * 10^{-6} \ \frac{Nm^3}{s} = 21.48 \ \frac{Nl}{h} \tag{15}$$

Further calculations are done under the assumption, that CO_2 hydrogenation to MeOH is the only reaction with decreasing number of molecules occurring in the reactor. The ratio of molecules of MeOH produced to total molecules attributing to volume decrease can be therefore estimated as:

$$ratio_{MeOH} = 0.5$$

Under the assumptions listed above, the volumetric rate of produced MeOH can be estimated as:

$$v_{MeOH} = v_{decrease} * ratio_{MeOH} = \ 2.984 * 10^{-6} \ \frac{Nm^3}{s} \approx 10.7 \ \frac{Nl}{h} \tag{16}$$

$$N_{MeOH} = v_{MeOH} * vol_m = \ 1.3 * 10^{-4} \ \frac{moles}{s} \tag{17}$$

Based on these results, as well as the volume and composition of process gas supplied to the reactor, the percent MeOH yield can be calculated:

$$\%Yield_{MeOH} = \frac{v_{MeOH}}{v_{CO2, \ inlet}} * 100\% = \frac{10.74 \ \frac{Nl}{h}}{125 \ \frac{Nl}{h}} * 100\% \approx 8.6 \ \% \tag{18}$$

The enthalpy of the CO_2 hydrogenation reaction in the reactor operating conditions has the value of $\Delta H_{MeOH}(50 \ bar, \ \ 215°C) = -46.73 \ \frac{kJ}{mol}$.

CO_2 hydrogenation is, however, not the only reaction taking place in the reactor, and even in this reaction alone some steps are exothermic and some endothermic. However, with the aim of modelling heat generation in steady state operation of the reactor, it is possible to use the simple formula for total reaction heat generated in the reactor considering only CO_2 hydrogenation:

$$Q_{MeOH} = N_{MeOH} * \Delta \mathrm{H}_{\mathrm{MeOH}}(50\,bar,\ \ 215°C) = \\ = 1.332 * 10^{-4}\,\frac{moles}{s} * (-46.73) * 10^{3}\,\frac{J}{mol}\ \approx\ -6.2\,W \tag{19}$$

The value of Q_{MeOH} has been derived under several assumptions, of which the major one was that the reaction takes place in steady state conditions. In addition, this result is based on previously reported physics simplifications in the model and its aim is to provide a level of reference for researchers about the heat generation scale in the reactor. The numerical results obtained in this thesis are strongly affected by these simplifications, therefore being subjected to a range of error. This includes reaction heat, quantity of product molecules and product volume.

Figures 27-32 illustrate the results of simulations a), b), and c), conducted with the model presented in chapter 3.2, under the assumptions introduced earlier in chapter 4.2. In each of the figures, the temperature values simulated at *PT3* and *PT4* sensors are compared with experimental data from experiments a), b) and c). The X-axes of Figures 27-32 represent duration of simulations as time reference.

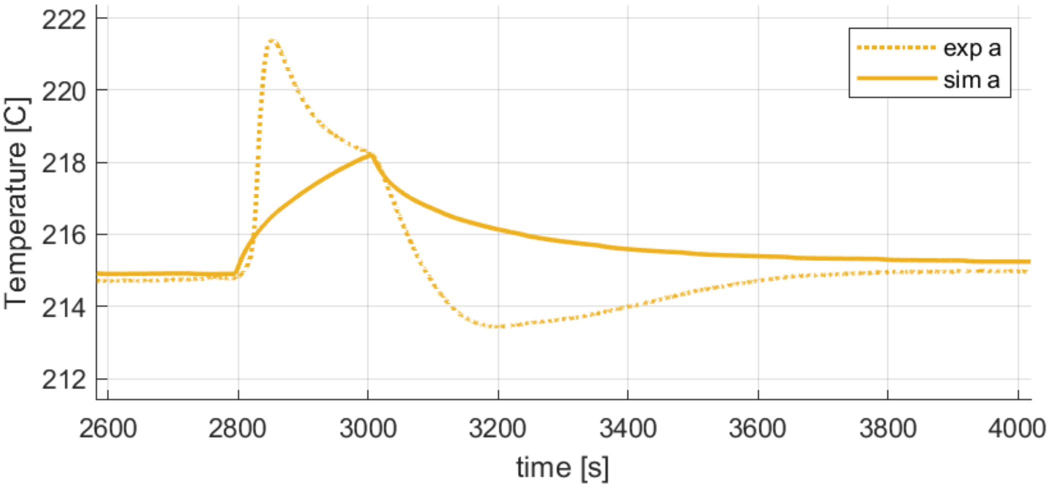

Figure 27: Comparison of *PT3* simulation a) results (solid lines) with experimental data (dotted lines).

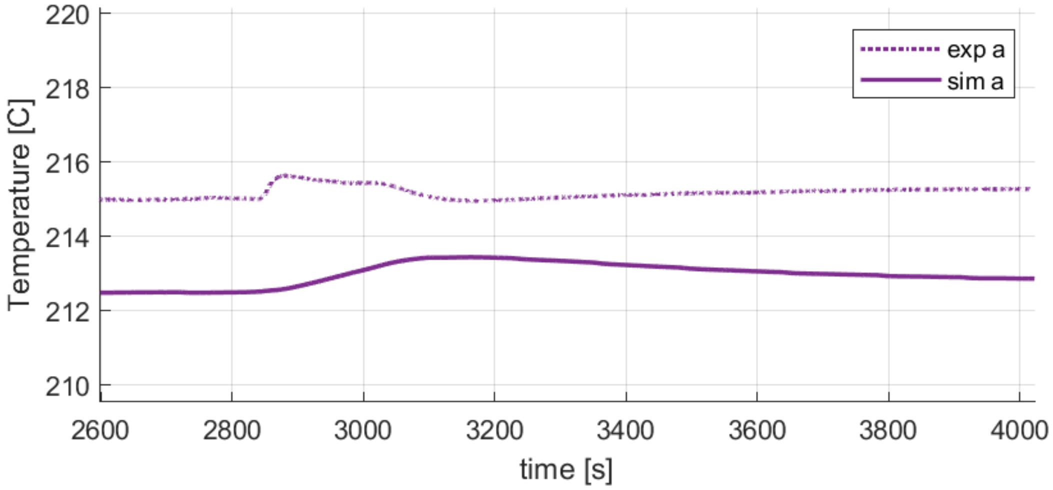

Figure 28: Comparison of *PT4* simulation a) results (solid lines) with experimental data (dotted lines).

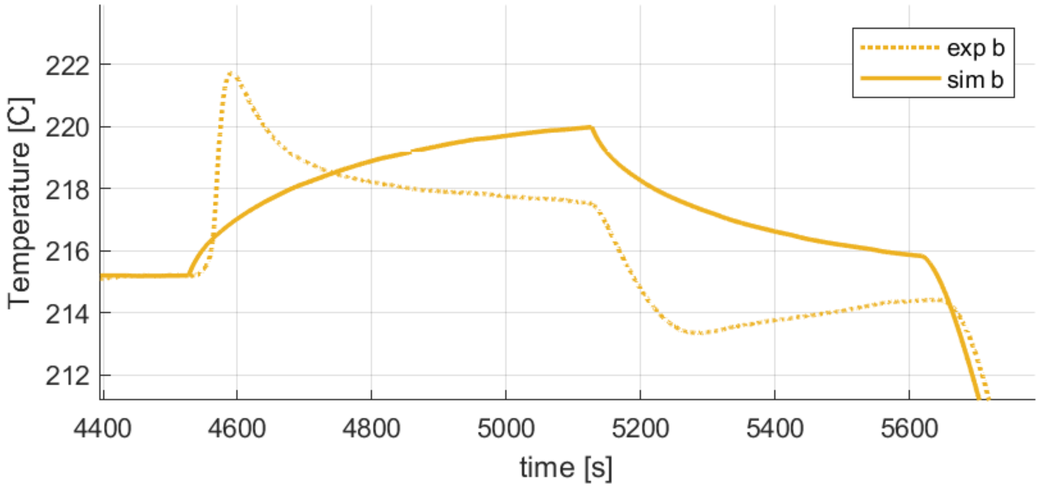

Figure 29: Comparison of *PT3* simulation b) results (solid lines) with experimental data (dotted lines).

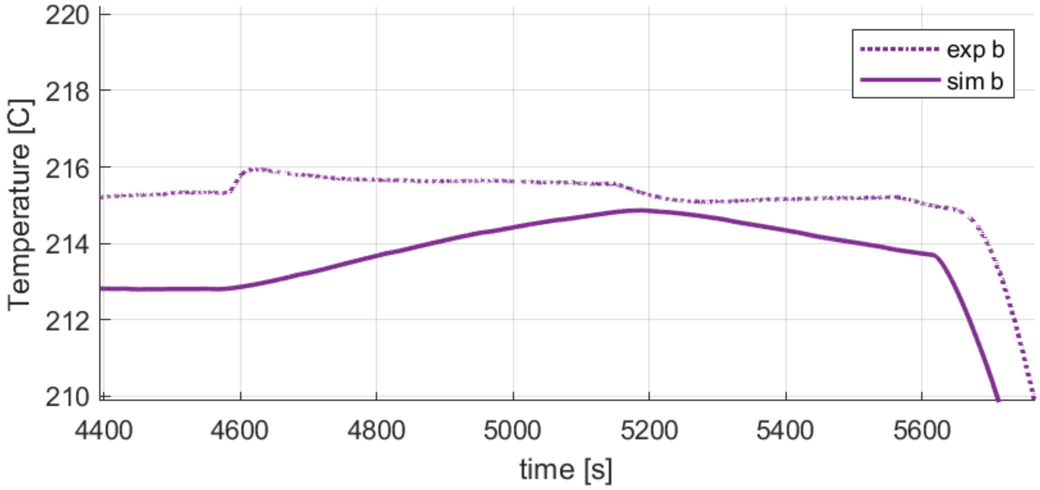

Figure 30: Comparison of *PT4* simulation b) results (solid lines) with experimental data (dotted lines).

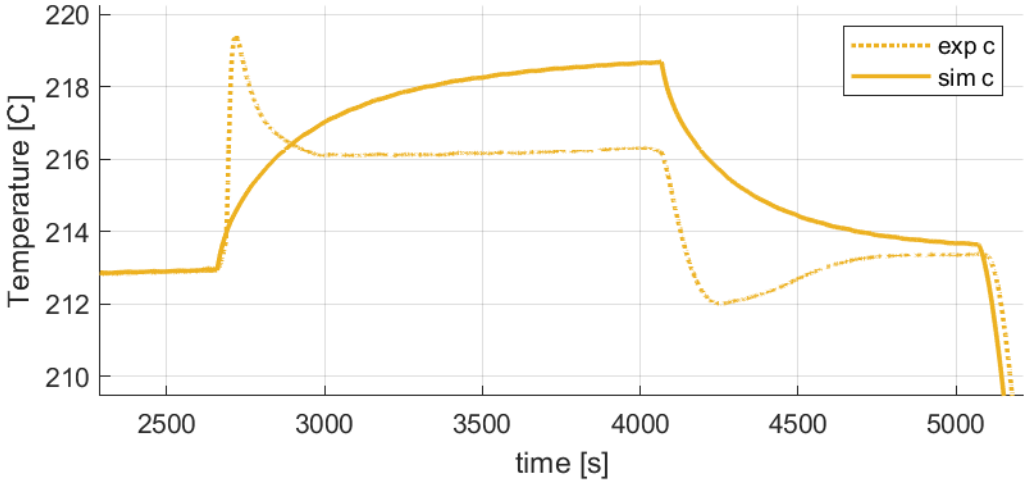

Figure 31: Comparison of *PT3* simulation c) results (solid lines) with experimental data (dotted lines).

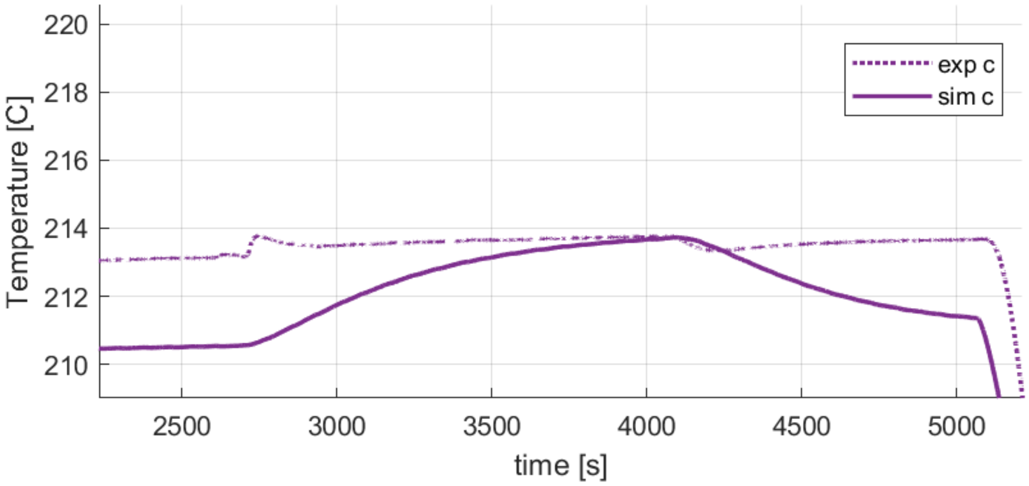

Figure 32: Comparison of *PT4* simulation c) results (solid lines) with experimental data (dotted lines).

In all of the simulations a), b), and c), the shapes of simulated *PT3* curves are significantly different from the experimental ones. These simulated curves resemble exponential functions in shape, which is a behaviour typical for a material being heated up by the heat source with constant heat flux. The curves lead towards stabilisation over time at a certain steady *PT3* values, indicating the balance of reaction heat generation flux with additional heat loss flux. Such balance has almost been reached during the longest of simulations: simulation c) shown in Figure 31. After the interruption of reactants inflow, the simulated *PT3* temperatures decreases to the prior steady state temperature, following asymptotic function shape

The differences of dynamics between simulated and experimental *PT3* temperatures in all three simulations are caused by modelling simplifications of reactor physics, described broadly in chapter 3.2. The modelling assumption of steady state heat generation through the whole duration of chemical reaction does not address changing reaction rate during different reaction steps, causing predominant exothermic behaviour during start-up and predominant endothermic behaviour during shut-down of the reactor. Thus, the most accurate representation of the thermal behaviour of the reactor is available only in a steady state operation timespans of the modelling simulations.

Simulated *PT4* curves are also not similar in shape to experimental curves in neither of the cases a), b), nor c). This is expected, as both in simulations and experiments, the shape of *PT4* curves reflects the diluted shape of *PT3* curves with a lower magnitude due to the effects of diffusion and advection. In simple terms, when both simulated and experimental *PT3* shapes are not similar to each other, then the *PT4* shapes are most likely not to be similar either.

The most important information obtained from the simulations is the maximum temperature level in different parts of the reactor. The maximum temperature errors during all of the simulations occur at the catalyst layer (*PT3*) during reactor start-up, approximately 1 min after injection of process gas. This takes place right after a rapid rise of experimental temperature caused by exothermicity of initial reaction steps. This maximum error's value was 6.4°C. The second highest temperature errors take place soon after the beginning of reactor shutdown, when experimental *PT3* values have declined faster than in simulations due to endothermicity of final reaction steps. At that moment, the error reached 3.9°C. For comparison, the errors at *PT4* remain under 3.9°C value during the whole time of all of the simulations. Overall, although the model's main application is simulation of the steady state operation of the reactor, the errors are at the level below 10°C even in dynamic operation stages. Such an order of accuracy allows to utilise the model introduced in this thesis as a tool for planning further experiments and assuring operational safety.

The values of *PT3* temperature in simulations and experiments in case c) (Figure 31), did not reach similar values despite almost reaching the steady state. In the simulation, *PT3* values stabilised at 218.7°C, while in the corresponding experiment, the steady state temperature reached 216.2°C. This is a notable difference, taking into account the perfect match of these curves at primary steady state temperature of 213°C before the injection of reactants. The change in the simulated steady state catalyst layer temperature after the reactor start-up is 5.7°C, while reaching only 3.2°C in the experiments. Although there are several sources, which partially contribute to this error, the main expected cause for such a substantial difference is the modelling of heat generation, which does not take into account other side chemical reactions, such as the RWGS reaction for the estimated value of total reaction heat during steady state operation.

Figures 33,34 present the results of further simulations marked as case d), which were conducted with the aim to find such a total reaction heat value $Q_{MeOH+RWGS}$, so that the simulated *PT3* temperature converged with the experimental *PT3* temperature of the experiment c) during steady state.

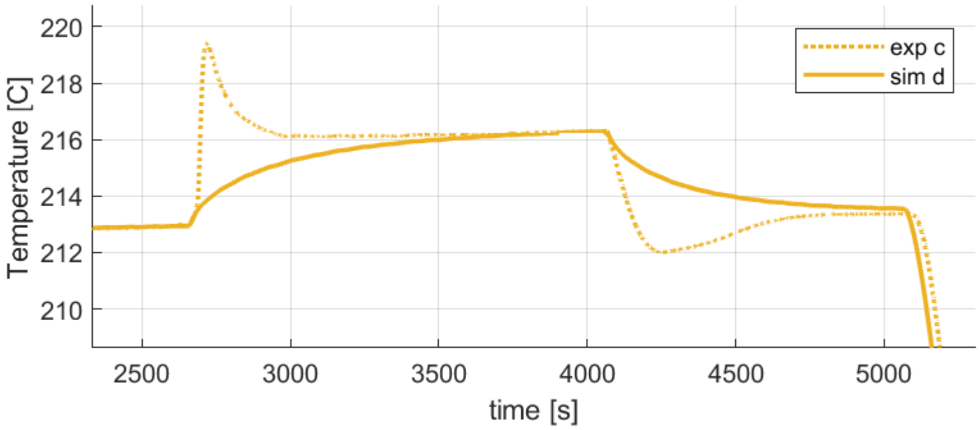

Figure 33: Comparison of *PT3* simulation d) results (solid lines) with experimental data from experiment c) (dotted lines). The results converge at steady state.

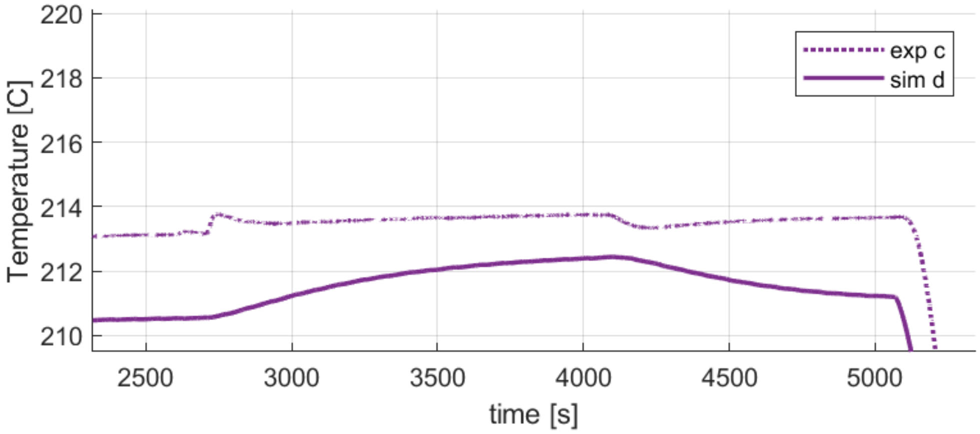

Figure 34: Comparison of *PT4* simulation d) results (solid lines) with experimental data from experiment c) (dotted lines).

Figure 33 shows the simulated *PT3* values under aforementioned assumptions, proving the condition of convergence between steady state *PT3* temperatures of simulation d) and experiment c). Simultaneously, the *PT4* temperature values from the same simulation reach the steady state difference of 1.5°C between the simulation d) and the experiment c).

The steady state reaction heat value, which was found to meet such a requirement, is:

$$Q_{MeOH+RWGS} = -3.5\ W$$

Under the assumption of attributing the total difference of reaction heat between Q_{MeOH} and $Q_{MeOH+RWGS}$ to RWGS reaction, the heat generated by this reaction can be estimated as:

$$Q_{RWGS} = Q_{MeOH+RWGS} - Q_{MeOH} = \\ -3.5 - (-6.22) \approx 2.7\ W \tag{20}$$

The enthalpy of the RWGS reaction in such operating conditions has the value of $\Delta \mathrm{H}_{\mathrm{RWGS}}(50\,bar,\ \ 215°C) = 47.02\,W.$

Based on the values of total RWGS reaction heat and its enthalpy of reaction, it is possible to estimate the volumetric flow rate of CO produced in a steady state reactor operation:

$$N_{CO} = \frac{Q_{RWGS}}{\Delta \mathrm{H}_{\mathrm{RWGS}}} = \frac{2.72\,W}{47.02 * 10^3 \frac{J}{mol}} \approx\ 5.8 * 10^{-5}\ \frac{mol}{s} \tag{21}$$

$$v_{CO} = \frac{N_{CO}}{vol_m} = \frac{5.78 * 10^{-5}\ \frac{mol}{s}}{44.643\ \frac{mol}{m^3 * bar}} = 1.3 * 10^{-6}\ \frac{Nm^3}{s} \approx 4.7\ \frac{Nl}{h} \tag{22}$$

All values calculated in this chapter, including reaction heat, quantity of product molecules, product volume and yield are estimates based on several assumptions and simplifications. These estimates serve as tools in the process of research, allowing to establish levels of reference and understand the scale of ongoing phenomena. The obtained results have value as an aid in experimental research, e.g., in originating hypotheses and proposals for further experiments, despite their numerical values being subjected to errors.

The model described in this thesis is a valuable tool to predict the thermal response of the experimental reactor, despite the fact that it does not simulate chemical reaction kinetics. Its advantages include simplicity and the pace of results generation. It takes a couple of seconds to compute the results of 1-hour long transient simulation in comparison to heavy duty CFD programs, which require long time spans to obtain such results. The most significant advantage of this model was that the simulation could be used as a function in a curve fitting regression process to obtain the experimentally derived heat transfer coefficients reported in chapter 4.1. The process of calibration of five different coefficients takes approximately 30 min.

5 Conclusions

Methanol is a chemical compound with a wide range of applications in the industry today. It is a feedstock in production processes of polymers, textiles, solvents, paints, pharmaceuticals, and many more products, which the civilisation relies on. However, current methanol production originates with fossil fuels. It means that when the materials produced from methanol at the end of their life are landfilled or incinerated, they release CO2, which is a greenhouse gas. With 2050 climate neutrality goals, it is necessary to replace the current supply chain of methanol with climate-neutral synthetic methanol, enabling the production of climate-neutral products. Methanol has also many appreciated properties for energy storage purposes, so it can be used as a fuel or fuel feedstock in several applications, such as marine transport or carbon neutral gas power plants equipped with carbon capture technology.

Methanol reactor synthesis through CO2 hydrogenation is a process, which still can be further improved. Switching from a currently favoured by industry two-step process of RWGS to CO hydrogenation to a process of direct CO2 hydrogenation could reduce the energy losses related to synthetic methanol production. However, these improvements require higher % yields to be achieved in power to methanol reactors. With the aim of achieving such improvements, more research on new catalysts and favourable reactor setups needs to be performed.

This thesis investigates the heat transfer phenomena occurring in the laboratory scale power to methanol reactor, which was designed and built at Aalto University to study methanol synthesis yields with different catalysts and reaction conditions. Experimental methods for measuring the conditions inside the reactor were reported, along with description of the instrumentation. A new CFD model for simulation of heat transfer was developed in order to enhance the measurements of the reactor's temperature and provide aid in planning future experiments. The developed model is heterogeneous, which means that although fixed bed space is represented in continuous form, two phases of catalyst particles and void space exist separately. The following implication is that both temperature data and thermal properties data are separately assigned to bed particles and to void space.

The model represents simplistic approach to modelling of the fixed bed reactors in comparison to existing particle-resolved 3D models existing in the literature. The result of that is less accurate representation of temperature distribution inside the reactor. Subsequently, the model does not include any representation of chemical reaction kinetics, but uses averaged volume heat generation approach to mimic heat of reactions. Although these simplifications affect the accuracy of temperature simulations, the model is characterised by very low computation cost. Due to explicit fluid kinematics and depicting chemical reactions as volumetric heat generation, the only equation solved across the mesh volumes is heat balance. In result, the model enables fast simulations of transient heat transfer of runs with tens of minutes of duration. The latter was particularly important in heat transfer coefficients calibration using regression, where many simulations needed to be performed.

The CFD model was calibrated with experimental data, resulting in estimation of heat transfer coefficients between several inter-material interfaces inside the reactor. The simulations achieved sufficient accuracy to help in experiment planning and reactor safety assessment, with the error being in the range of 10°C. The data of bed temperature acquired from experiments in transient conditions was used to investigate the chemical reaction behaviour of the power to methanol reactor during start up, steady state operation and shutdown.

The following reaction quantities were estimated based on the reactor's steady state operation in partial load:

Heat of CO2 hydrogenation to MeOH: $Q_{MeOH} = -6.2\ W$,
Heat of RWGS reaction: $Q_{RWGS} = 2.7\ \ W$,
Volumetric flow rate of MeOH product: $v_{MeOH} = 10.7\ \frac{Nl}{h}$,
Methanol product % yield: $\%Yield_{MeOH} = 8.6\ \%$,
Volumetric flow rate of methanol product: $v_{MeOH} = 10.7\ \frac{Nl}{h}$.

The results obtained in this thesis are subject to several limitations, including measurement errors and modelling simplifications. Measurement errors of some order exist every time an experiment is performed. However, in empirical models, such as the model introduced in this thesis, measurement errors also affect results of modelling. This is due to uncertainty propagation, which happens whenever model parameters are fitted with experimental data. Modelling simplification such as heterogeneous bed representation, coarse meshing or explicit conditions for fluid kinematics also affect the model's precision.

The obtained value of heat transfer coefficient between fluid and bed particles had a relatively very high value of $c_{fb} = 100\ \frac{W}{K}$, which was at the boundary of specified limits. This means that the heat transfer between these media was assumed as nearly instantaneous, while the temperature difference was in all cases negligible. A conclusion from this is that in this case it would not make any difference if the developed model was homogeneous, instead of heterogeneous. Such an approach could further reduce the model complexity.

Advances in CFD and other modelling methods in recent years are significant and allow for multi-level reactor modelling. However, aside from high precision simulations, there are also situations, when there is a preference for simplistic approaches, such as homo or heterogeneous models due to their shorter development time and low demand of computational power. Complexity of calculations is always accompanied with corresponding computational cost, therefore a proper method must be carefully chosen. In particular case of the power to methanol reactor reported in this thesis, the presented model can be further improved by mesh refinement with adding more radial layers, in order to create a representation of radial distribution of temperature. Another prospective improvement could be the inclusion of simple macrokinetics modelling, such as power law kinetics. These improvements would lead to better representation of the multiphysical phenomena occurring in the reactor, while retaining relative simplicity of the model. When it comes to reactor design optimisation, more rigorous models are recommended for that purpose, in order to include a detailed internal structure of the fixed bed into simulations. One of the prospective approaches to develop such a model would be to create a 3D particle resolved CFD and combine it with kinetic models derived from DFT studies on reaction mechanisms.

References

[1] Intergovernmental Panel on Climate Change (IPCC), “Climate Change 2022 Impacts, Adaptation and Vulnerability,” IPCC, Switzerland, 2022.

[2] R. Dellink, “Towards global carbon pricing: Direct and indirect linking of carbon markets.,” *OECD Journal: Economic Studies,* vol. 2013/1, 2014.

[3] M. Crippa, D. Guizzardi, E. Solazzo, M. Muntean, E. Schaaf and F. Monforti-Ferrario, “GHG emissions of all world countries - 2021 Report,” Publications Office of the European Union, Luxembourg, 2021.

[4] IRENA, “Power System Flexibility for the Energy Transition, Part 1: Overview for policy makers,” International Renewable Energy Agency, Abu Dhabi, 2018.

[5] R. P. Lee, “Alternative carbon feedstock for the chemical industry? - Assessing the challenges posed by the human dimension in the carbon transition,” *Journal of Cleaner Production,* vol. 219, pp. 786-796, 2019.

[6] A. Basile and F. Dalena, Methanol : science and engineering. Methanol, ed. F. Dalena. 2018: Amsterdam,, Amsterdam: Elseviewer, 2018.

[7] Olah, A. Goeppert and G. K. S. Prakash, Beyond oil and gas : the methanol economy., Wiley-VCH, 2018.

[8] P. Kluesener, I. Pyc and G. Zimmermann, “e-Methanol - A universal green fuel,” Siemens Energy Global GmbH & Co. KG, 2021.

[9] M. Bertau, H. Offermanns, L. Plass, F. Schmidt and H. Wernicke, Methanol: The Basic Chemical and Energy Feedstock of the Future, Springer, 2014.

[10] Haldor Topsoe, “Methanol for a more sustainable future,” Haldor Topsoe , [Online]. Available: https://info.topsoe.com/hubfs/DOWNLOADS/DOWNLOADS%20-%20Brochures/eMethanol.pdf?hsCtaTracking=6ca24cee-0aed-45df-8aa4-846ecd19151c%7C5d9f6bef-ebfc-483e-8a06-cdfed4aee34a. [Accessed 2022 July 9].

[11] IRENA AND METHANOL INSTITUTE, “Innovation Outlook : Renewable Methanol,” International Renewable Energy Agency, Abu Dhabi, 2021.

[12] F. Pontzen, W. Liebner, V. Gronemann, M. Rothaemel and B. Ahlers, "CO2-based methanol and DME – Efficient technologies for industrial scale production," *Catalysis Today,* vol. 171, no. 1, p. 242–250.

[13] A. Santasalo-Aarnio, J. Nyari, M. Wojcieszyk, O. Kaario and J. Kroyan, "Application of Synthetic Renewable Methanol to Power the Future Propulsion," *SAE Technical Papers,* 2020.

[14] Carbon Recycling International, "Our projects: Carbon Recycling International," Carbon Recycling International, [Online]. Available: https://www.carbonrecycling.is/projects#project-goplant. [Accessed 07 07 2022].

[15] Celanese Corporation , "Celanese to Expand Capacity and Utilize Recycled CO2 for Methanol Production at Clear Lake, Texas Facility," Irving, Texas, 2021.

[16] J. Nyári, M. Magdeldin, M. Larmi, M. Järvinen and A. Santasalo-Aarnio, "Techno-economic barriers of an industrial-scale methanol CCU-plant," *Journal of CO2 Utilization,* vol. 39, 2020.

[17] A. Dixon, M. Nijemeisland and E. Stitt, "Dixon, A.G., Nijemeisland, M., & Stitt, E.H. (2006). Packed Tubular Reactor Modeling and Catalyst Design using Computational Fluid Dynamics," *Advances in Chemical Engineering,,* vol. 31, pp. 307-389, 2006.

[18] G. Wehinger, "Particle-resolved CFD simulations of catalytic flow reactors. Doctoral dissertation," *Fakultät III - Prozesswissenschaften der Technischen Universität Berlin,* 2016.

[19] M. U. Bohnet, Fixed Bed Reactors - Ullmann's Encyclopedia of Industrial Chemistry, Wiley VCH, 2003.

[20] J. Lange, "Methanol synthesis: a short review of technology improvements," *Catalysis Today,* vol. 64, pp. 3-8, 2001.

[21] R. Dry, "Possibilities for the development of large-capacity methanol synthesis reactors for synfuel production," *Industrial & Engineering Chemistry Research,* vol. 27, no. 4, p. 616–624, 1988.

[22] N. Jurtz, M. Kraume and G. Wehinger, "Advances in fixed-bed reactor modeling using particle-resolved computational fluid dynamics (CFD)," *Reviews in Chemical Engineering,* vol. 35(2), p. 139–190, 2019.

[23] T. Eppinger, G. Wehinger, N. Jurtz, R. Aglave and M. Kraume, "A numerical optimization study on the catalytic dry reforming of methane in a spatially resolved fixed-bed reactor," *Chemical Engineering Research and Design , . 10th European Congress,* vol. 115, no. Part B, p. 74–381, 2016.

[24] J. Yang, Q. Wang, M. Zeng and A. Nakayama, “Computational study of forced convective heat transfer in structured packed beds with spherical or ellipsoidal particles,” *Chemical Engineering Science,* vol. 65, pp. 726-738, 2010.

[25] P. Arce and D. Ramkrishna, “Pattern formation in catalytic reactors: the role of fluid mixing,” *American Institute of Chemical Engineers (AIChe) Journal,* vol. 37, no. 1, pp. 98-110, 1991.

[26] D. Izbassarov, J. Nyari, B. Tekgul, E. Laurila and T. Kallio, “A numerical performance study of a fixed-bed reactor for methanol synthesis by CO2 hydrogenation,” *International Journal of Hydrogen Energy,* vol. 46, pp. 15635-15648, 2021.

[27] M. Elsari and R. Hughes, “Axial effective thermal conductivities of packed beds,” *Applied Thermal Engineering,* vol. 22, p. 1969–1980, 2002.

[28] V. Hlavacek, J. Puszynski, H. Viljoen and J. Gatica, Model Reactors and Their Design Equations - Ullmann’s Encyclopedia of Industrial Chemistry, Wiley VCH, 2003.

[29] A. P. De Wasch and G. F. Froment, “A two dimensional heterogeneous model for fixed bed catalytic reactors,” *Chemical Engineering Science,* vol. 26, pp. 629-634, 1971.

[30] R. Wijngaarden and K. Westerterp, “A heterogeneous model for heat transfer in packed beds,” *Chemical Engineering Science,* vol. 48, no. 7, pp. 1273-1280, 1993.

[31] Z. Nawaz, “Heterogeneous Reactor Modeling of an Industrial Multitubular Packed-Bed Ethylene Oxide Reactor,” *Chemical Engineering Technology,* 2016.

[32] F. Manenti, S. Cieri and M. Restelli, “Considerations on the steady-state modeling of methanol synthesis fixed-bed reactor,,” *Chemical Engineering Science,* vol. Volume 66, no. Issue 2, pp. 152-162, 2011.

[33] M. Müller, M. Kutscherauer, S. Böcklein, G. Wehinger, T. Turek and G. Mestl, “Modeling the selective oxidation of n-butane to maleic anhydride: From active site to industrial reactor,” *Catalysis Today,* vol. 387, pp. 82-106, 2022.

[34] G. Wehinger, F. Klippel and M. Kraume, “Modeling pore processes for particle-resolved CFD simulations of catalytic fixed-bed reactors,” *Computers & Chemical Engineering,* vol. 101, pp. 11-22, 2017.

[35] E. Moghaddam, E. Foumeny, A. Stankiewicz and J. Padding, “Multiscale modelling of wall-to-bed heat transfer in fixed beds with non-spherical pellets: From particle-resolved CFD to pseudo-

homogenous models,," *Chemical Engineering Science,,* vol. 236, 2021.

[36] Z. Minhua, D. He and G. Zhongfeng, "A particle-resolved CFD model coupling reaction-diffusion inside fixed-bed reactor," *Advanced Powder Technology,* pp. 1226-1238, 2019.

[37] X. Yang, T. Scheibe, M. Richmond, W. Perkins, S. Vogt and S. Codd, "Direct numerical simulation of pore-scale flow in a bead pack: comparison with magnetic resonance imaging observations.," *Advances in Water Resources,* vol. 54, p. 228–241, 2013.

[38] M. Baker, "CFD simulation of flow through packed beds using the finite volume technique.," *PhD Thesis, University of Exeter,* 2011.

[39] G. Dixon, E. Taskina, M. Nijemeislandb and S. H.E., "Wall-to-particle heat transfer in steam reformer tubes: CFD comparison of catalyst particles," *Chemical Engineering Science,* vol. 63, p. 2219 – 2224, 2008.

[40] R. Caulkin, X. Jia, M. Fairweather and R. Williams, "Predictions of Porosity and Fluid Distribution Through Nonspherical-Packed Columns," *American Institute of Chemical Engineers (AIChe) Journal,* vol. 58, no. 5, pp. 1503-1512, 2011.

[41] M. Marek, "Numerical generation of a fixed bed structure," *Chemical and Process Engineering,* vol. 34, no. 3, pp. 347-359, 2013.

[42] S. Flaischlen and G. Wehinger, "Synthetic Packed-Bed Generation for CFD Simulations: Blender vs. STAR-CCM+," *ChemEngineering,* vol. 3, no. 2, 2019.

[43] C. R., J. X., X. C., F. M. and R. A. Williams, "Simulations of Structures in Packed Columns and Validation by X-ray," *Industrial & Engineering Chemistry Research,* vol. 48, pp. 202-213, 2009.

[44] H. Bai, J. Theuerkauf and P. Gillis, "A Coupled DEM and CFD Simulation of Flow Field and Pressure Drop in Fixed Bed Reactor with Randomly Packed Catalyst Particles," *Industrial & Engineering Chemistry Research,* vol. 48, no. 8, pp. 4060-4074, 2009.

[45] T. Eppinger, G. Wehinger and M. Kraume, "Parameter optimization for the oxidative coupling of methane in a fixed bed reactor by combination of response surface methodology and computational fluid dynamics.," *Chemical Engineering Research and Design,* vol. 92, pp. 1693-1703, 2014.

[46] Moukalled, L. Mangani and M. Darwish, The finite volume method in computational fluid dynamics : an advanced introduction with OpenFOAM and Matlab, Springer, 2015.

[47] M. Peric, “Flow simulation using control volumes of arbitrary polyhedral shape,” in *ERCOFTAC Bulletin 62*, 2004.

[48] M. Salciccioli, M. Stamatakis, S. Caratzoulas and D. Vlachos, “A review of multiscale modeling of metal-catalyzed reactions: Mechanism development for complexity and emergent behavior,” *Chemical Engineering Science,* vol. 66, pp. 4319-4355, 2011.

[49] M. Orio, A. Pantazis and F. Neese, “Density functional theory,” *Photosynthesis Research,* vol. 102, p. 443–453, 2009.

[50] E. E. and D. R. M., Density Functional Theory: An Advanced Course, Berlin: Springer, 2011.

[51] K. Ushikoshi, K. Mori, T. Kubota, T. Watanabe and M. Saito, “Methanol synthesis from CO_2 and H_2 in a bench-scale test plant,” *Applied Organometallic Chemistry,* vol. 14, no. 12, pp. 819 - 825, 2000.

[52] G. Bozzano and F. Manenti, “Efficient methanol synthesis: Perspectives, technologies and optimization strategies,” *Progress in Energy and Combustion Science,* vol. 56, pp. 71-105, 2016.

[53] M. Takagawa and M. Ohsugi, “Study on reaction rates for methanol synthesis from carbon monoxide, carbon dioxide, and hydrogen,” *Journal of Catalysis,* vol. 107, no. 1, pp. 161-172, 1987.

[54] P. Villa, P. Forzatti, G. Buzzi-Ferraris, G. Garone and I. Pasquon, “Synthesis of alcohols from carbon oxides and hydrogen. Kinetics of the low-pressure methanol synthesis.,” *Industrial & Engineering Chemistry Process Design and Development,* 1985.

[55] M. Setinc and J. Levec, “Dynamics of a mixed slurry reactor for the three-phase methanol synthesis.,” *Chemical Engineering Science,* vol. 56, no. 21-22, pp. 6081-6087, 2001.

[56] K. Vanden Bussche and G. Froment, “A steady-state kinetic model for methanol synthesis and the water gas shift reaction on a commercial $Cu/ZnO/Al_2O_3$ catalyst,” *Journal of Catalysis,* vol. 161, no. 1, pp. 1-10, 1996.

[57] G. Graaf, E. Stamhuis and A. Beenackers, “Kinetics of low-pressure methanol synthesis,” *Chemical Engineering Science,* vol. 43, no. 12, pp. 3185-3195, 1988.

[58] H. P. M. K. S. C. H. B. J. J. K. Lim, “Modeling of the Kinetics for Methanol Synthesis using $Cu/ZnO/Al_2O_3/ZrO_2$ Catalyst: Influence of Carbon Dioxide during Hydrogenation,” *Industrial & Engineering Chemistry Research,* vol. 48, no. 23, pp. 10448-10455, 2009.

[59] G. Chinchen, C. Hay, H. Vandervell and K. Waugh, "The measurement of copper surface areas by reactive frontal chromatography," *Journal of Catalysis,* vol. 103, pp. 79-86, 1987.

[60] G. Liu, D. Willcox, M. Garland and H. Kung, "The role of CO2 in methanol synthesis on Cu/Zn oxide: An isotope labeling study," *Journal of Catalysis,* vol. 96, pp. 251-260, 1985.

[61] G. Graaf, H. Scholtens, E. Stamhuis and A. Beenackers, "Intra-particle diffusion limitations in low-pressure methanol synthesis," *Chemical Engineering Science,* vol. 45, no. 4, pp. 773-783, 1990.

[62] I. B. Dybkjær, "Design of Ammonia and Methanol Synthesis Reactors," *Chemical Reactor Design and Technology,* p. 795–819, 1986.

[63] K. Klier, V. Chatikavanij, R. Herman and G. Simmons, "Catalytic synthesis of methanol from COH2: IV. The effects of carbon dioxide," *Journal of Catalysis,* vol. 74, no. 2, pp. 343-360, 1982.

[64] T. Askgaard, J. Norskov, C. Ovesen and P. Stoltze, "A Kinetic Model of Methanol Synthesis," *Journal of Catalysis,* vol. 156, no. 2, pp. 229-242, 1995.

[65] C. Ovesen, B. Clausen, J. Schiøtz, P. Stoltze, H. Topsøe and J. Nørskov, "Journal of Catalysis," *Kinetic Implications of Dynamical Changes in Catalyst Morphology during Methanol Synthesis over Cu/ZnO Catalysts,* vol. 168, no. 2, pp. 133-142, 1997.

[66] L. C. Grabow and M. Mavrikakis, "Mechanism of Methanol Synthesis on Cu through CO2and CO Hydrogenation," *ACS Catalysis,* vol. 1, no. 4, p. 365–384, 2011.

[67] N. Park, M. Park, Y. Lee, K. Ha and K. Jun, "Kinetic modeling of methanol synthesis over commercial catalysts based on three-site adsorption," *Fuel Processing Technology,* vol. 125, pp. 139-147, 2014.

[68] N. Park, M. Park, K. Ha, Y. Lee and K. Jun, "Modeling and analysis of a methanol synthesis process using a mixed reforming reactor: Perspective on methanol production and CO2 utilization," *Fuel,* vol. 129, pp. 163-172, 2014.

[69] H. Lim, M. Park, S. Kang, H. Chae, J. Bae and K. Jun, "Modeling of the Kinetics for Methanol Synthesis using Cu/ZnO/Al2O3/ZrO2 Catalyst: Influence of Carbon Dioxide during Hydrogenation," *Industrial & Engineering Chemistry Research,* vol. 48, no. 23, pp. 10448-10455, 2009.

[70] M. Laitinen, "An experimental setup for methanol production for renewable," *Master's thesis of Aalto University,* 2020.

[71] O. R. Derkx and A. G. & Dixon, “Determination of the fixed bed wall heat transfer coefficient using computational fluid dynamics. Numerical heat transfer,” *An International Journal of Computation and Methodology,,* vol. 29, no. 8, pp. 777-794, 1996.

[72] C. Berto and G. Barreto, “The relevance of overall heat transfer coefficients in the simulation of catalytic fixed bed reactors with the heterogeneous one-dimensional model,” *Applied Mathematical Modelling,* vol. 16, no. 10, pp. 520-533, 1992.

[73] C. O. Castillo-Araiza, H. Jiménez-Islas and F. López-Isunza, “Heat-Transfer Studies in Packed-Bed Catalytic Reactors of Low Tube/Particle Diameter Ratio,” *Industrial & Engineering Chemistry Research,* vol. 46, no. 23, p. 7426–7435, 2007.

[74] A. Zenner, K. Fiaty, V. Bellière-Baca, C. Rocha, G. Gauthier and D. Edouard, “Effective heat transfers in packed bed: Experimental and model investigation,” *Chemical Engineering Science,* vol. 201, pp. 424-436, 2019.

[75] D. Geb, F. Zhou and I. Catton, “Internal Heat Transfer Coefficient Determination in a Packed Bed From the Transient Response Due to Solid Phase Induction Heating,” *Journal of Heat Transfer,* vol. 134, no. 4, 2012.

[76] L. Murray and E. Reiff, “Design of transient experiments for identification of fixed bed thermal transport properties,” *Canadian Journal of Chemical Engineering,* vol. 62, no. 1, pp. 55-61, 1984.

[77] L. M. M. Jorge, R. M. M. Jorge, F. Fujii and G. R., “Evaluation of heat transfer in a catalytic fixed bed reactor at high temperatures,” *Brazilian Journal of Chemical Engineering,* vol. 16, no. 4, 1999.

[78] D. Nemec and J. Levec, “Flow through Packed Bed Reactors: 1. Single-Phase Flow,” *Chemical Engineering Science,* vol. 60, 2005.